

High-resolution velocity measurements on fully identified light nuclides produced in $^{56}\text{Fe} + \text{hydrogen}$ and $^{56}\text{Fe} + \text{titanium}$ systems

P. Napolitani^{1,2,*}, K.-H. Schmidt², A.S. Botvina^{2,3}, F. Rejmund^{1†}, L. Tassan-Got¹ and C. Villagrasa⁴

¹ *IPN Orsay, IN2P3, 91406 Orsay, France*

² *GSI, Planckstr. 1, 64291 Darmstadt, Germany*

³ *Inst. for Nuclear Research, Russian Academy of Sciences, 117312 Moscow, Russia and*

⁴ *DAPNIA/SPhN CEA/Saclay, 91191 Gif sur Yvette, France*

(Dated: July 11, 2018)

New experimental results on the kinematics and the residue production are obtained for the interactions of ^{56}Fe projectiles with protons and $^{\text{nat}}\text{Ti}$ target nuclei, respectively, at the incident energy of 1 A GeV. The titanium-induced reaction serves as a reference case for multifragmentation. Already in the proton-induced reaction, the characteristics of the isotopic cross sections and the shapes of the velocity spectra of light residues indicate that high thermal energy is deposited in the system during the collision. In the $^{56}\text{Fe}+p$ system the high excitation seems to favour the onset of fast break-up decays dominated by very asymmetric partitions of the disassembling system. This configuration leads to the simultaneous formation of one or more light fragments together with one heavy residue.

PACS numbers: 25.40.Sc, 25.70.Pq, 24.10.-i, 21.10.Gv

I. INTRODUCTION

For the last decades, the investigation of the maximum excitation energy that a nuclear system can hold has remained as much a challenge as the description of the decay of a hot collision remnant, excited beyond the limits of nuclear binding. It is commonly assumed that other decay modes than fission and evaporation prevail at high excitation energy. These modes are often described as a simultaneous break-up of the hot system in many parts, named “multifragmentation”. The excitation energy above which multifragmentation appears is still a source of intense theoretical and experimental research. A point of particular interest is to recognise the distinguishing traits denoting this decay mode when the excitation is just sufficient for its onset. In line with this investigation, one foremost aspect of intense discussion is the connection of the kinematics of the residues to the kind of equilibration process involved in the earliest stages of the decay. This question is related to the complementary effort in constructing physical models to deduce the formation cross sections of the residues when the excitation energy of the system is taken as initial condition. Especially light residues are suited for this purpose. Several details of the deexcitation mechanism could emerge from the kinematics of light fragments, due to the high sensitivity in probing the Coulomb field of the decaying system. Moreover, the distribution of their isotopic cross sections carry additional signatures connected to different decay modes.

The experimental data exploited in this work are part of a vast experimental campaign devoted to the collection of nuclear data for the design of accelerator-driven subcritical reactors [1] and to the investigation of spallation reactions in the cosmos [2]. The full set of production cross sections and fragment mean recoil velocities measured in this framework for the reaction $^{56}\text{Fe}+p$ and $^{56}\text{Fe}+^{\text{nat}}\text{Ti}$ at energies ranging from 300 to 1500 MeV is presented elsewhere [3].

A. The formation of light residues

Light residues can be generated in several kinds of processes. One of these, the binary decay of an excited greatly thermalised complex, named compound nucleus, was widely studied [4]. We might also recall that evaporation of nucleons and light nuclei and symmetric fission are just the opposite extremes of the manifestation of this process: there is a gradual transition from very asymmetric to symmetric configurations in the division of decaying compound nuclei, and thus all binary decays of a greatly thermalised system can be named fission in a generalized sense. This generalization was introduced by Moretto [5, 6]. A compound system far below the Businaro-Gallone point [7, 8] (like iron-like nuclei) undergoes very asymmetric fission, resulting in a characteristic U-shape in the mass distribution of the yields. A minimum located at symmetry in the yield mass spectrum corresponds to a maximum placed at symmetry in the ridge lines of the potential. In configurations where a heavy partner is present, the whole decay process is dominated by the binary decay, and an additional evaporation of single nucleons would not disturb the kinematics remarkably. Such a process exhibits the typical feature of the population of the shell of a sphere in velocity space, in the reference frame of the mother nucleus.

*This work forms part of the PhD thesis of P. Napolitani, Université Paris XI, Paris 2004, n.7620, preprint IPNO-T-04-14

†On departure to GANIL, Blvd. H. Becquerel, B.P. 5027, 14076 Caen, France

At high excitation, multifragmentation becomes the competing process to compound-nucleus reactions. There is a fundamental difference between the binary decay of a compound nucleus and the simultaneous disintegration of a hot collision remnant in several constituents. The difference is in the kind of instabilities which are the reason for the decay, and is reflected in the kind and in the time evolution of the consequent equilibration process followed by the system.

A hot nucleus with an excitation energy above the threshold for emission of particles or clusters (including fission) has the possibility to decay by any of the open channels. If the excited system is not too hot, the favoured process is a reordering of its configurations: a great number of arrangements are available where all nucleons remain in states below the continuum, occupying excited single-particle levels around the Fermi surface. Oscillations in fission direction are included in this picture as well, but too rarely the fission barrier is reached. Rather seldom, compared with this thermal chaotic motion of the system, one nucleon acquires enough energy to pass above the continuum and may eventually leave the nucleus. This picture might be extended to cluster decay and to fission. Since this decay is a rare process, one evaporation event, or fission event, proceeds after the other, sequentially. In this process, the compound system follows a dynamic trajectory in deformation space, which is governed by the potential-energy surface and the dynamic properties of the compound system, related, for instance, to the inertia tensor and dissipation tensor. All decays are binary.

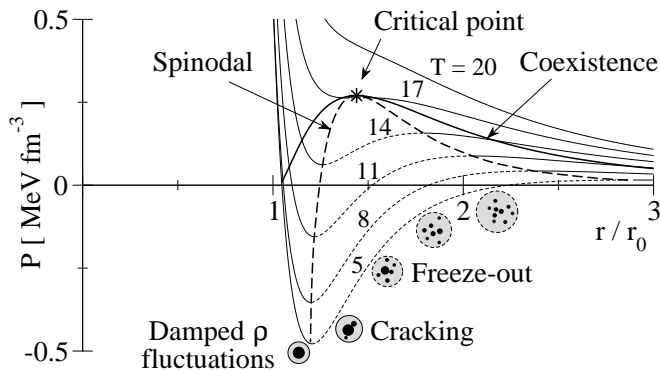


FIG. 1: Idealistic plot of the phase diagram of nuclear matter, deduced from a Skyrme force ([27] parameterised according to [28]). Pressure is shown as a function of the average relative nucleon distance r normalized to the distance r_0 at ground state. System configurations are drawn as possible final results of the expansion phase. When the thermalization path leads to the coexistence region, out of the spinodal region, damped density fluctuations occur. In the spinodal region density fluctuations are unstable and lead to cracking. At low density freeze-out is attained with different possible partition configurations: fragments are free to leave the system.

If the system becomes drastically more unstable, this picture is not valid anymore. The exploration of possible states of the excited system includes numerous unstable configurations. Thus, the disintegration can not be understood as a sequence of binary decays, but rather portrayed as a simultaneous break-up in several constituents [9, 10, 11, 12, 13]. The disintegration is simultaneous in the sense that it evolves in so short a time interval (10^{-22} - 10^{-21} s) that the ejected fragments can still exchange mutual interactions during their acceleration in the Coulomb field of the system. In heavy-ion collisions, part of the excitation could be introduced in the system in the form of compressional energy. According to the impact parameter and the incident energy, the interaction might result in a very complex interplay between dynamic effects (beside compression, also deformation and rotation degrees of freedom) and thermal excitation. This is the case of central collisions in the Fermi-energy range. On the contrary, peripheral heavy-ion collisions at relativistic energies may be rather pictured according to an “abrasion” process [14, 15], where the remnant is formed by the spectator nucleons, heated by mainly thermal energy. In this case, the role of compressional energy has minor incidence. Even with proton projectiles, the multifragmentation regime might be accessible when very high excitation is introduced in the nucleus. In reactions induced by relativistic protons (but also by very light nuclei), the dynamic effects of the collision have even smaller importance. The excitation energy is almost purely thermal. Some authors even attributed the specific name of “thermal multifragmentation” to this particular process (see the review articles [16, 17]). It might be suggested that proton-induced relativistic collisions are better suited than ion-ion collisions for investigating thermal properties of nuclear matter (e.g. [16, 18, 19, 20, 21]). In finite nuclei, the transition from the fission-evaporation mode to multifragmentation manifests rather smoothly. This opening of break-up channels even inspired interpretations in line with the liquid-gas phase transition of nuclear matter [22, 23, 24, 25]. The similarity of the nucleon-nucleon interaction with the Lennard-Jones molecular potential suggests that infinite neutral nuclear matter resembles a Van-der-Waals fluid [26]. As shown in fig. 1, also in the phase diagram of nuclear matter an area of liquid-gas coexistence can be defined. In this region, the “dense” phase of nuclear droplets is in equilibrium with the “gaseous” phase of free nucleons and light complex particles. Within the Hartree-Fock approximation, according to the type of Skyrme force chosen for obtaining the nuclear equation of state, the critical temperature T_c was calculated to vary in a range of around 15 to 20 MeV for nuclear matter [26, 27, 28]. (One of the latest investigations, based on an improved Fisher’s model [29] indicated $T_c = 6.7 \pm 0.2 \text{ MeV}$ for finite nuclear systems. This value is source of controversy, e.g. [17, 30]). During the reaction process, the system explores different regions of the phase diagram. Since at relativistic en-

ergies the collision is related to short wavelengths, the hot remnant should reach high positive values of pressure P due to thermal energy (rather than mechanical compression, characteristic of Fermi-energy collisions) without deviating sensibly from the initial density ρ_0 . It is commonly assumed that at this stage the system is still not thermalised and it undergoes expansion in order to attain equilibrium (There exist also opposite interpretations assuming thermalization already before expansion and a successive “Big-Bang-like” expansion out of equilibrium [31]). If the initial pressure is high enough, the subsequent expansion could lead to rather low densities, and the system, after dissipating the incoming momentum, could reach a point belonging to the spinodal region. Due to the inverse relation between pressure and density $dP/d\rho < 0$, this region is unstable, and density fluctuations are magnified. The nucleus breaks apart due to spinodal instability. The system disassembles also due to Coulomb instability. The inclusion of the long-range Coulomb interaction in the equation of state was introduced by Levit and Bonche [28], with the result that the solution of the coexistence equation vanishes above a “limiting temperature” T_{lim} , in general much lower than T_c , depending on the conditions taken for the calculation (see also [32, 33]). Density fluctuations reflect a continuous evolution of the size and number of nuclear droplets from a configuration to another [34]. If the average mutual distance among the nucleons exceeds the strong nuclear interaction range (i.e. about $\sqrt{\langle \sigma_n \rangle / \pi}$, where $\langle \sigma_n \rangle$ is the average nucleon-nucleon collision cross section), the break-up configuration “freezes” and the formed nuclei and nucleons fly away freely, all carrying signatures of the so-called freeze-out temperature of their common source. From comparing results from different experimental approaches e.g. [18, 24, 35, 36] this temperature is found to be restricted to a range of 5 to 6 MeV (corresponding to a range of excitation energy per nucleon around 2.5 to 3.5 MeV), quite independently of the reaction. This finding, not directly compatible with the phase diagram of ideal nuclear matter even suggested to search for a “characteristic temperature” of fragmentation [37]. The break-up configuration at freeze-out is expected to reflect the excitation energy of the system. The dense phase of highly heated systems should have the aspect of an ensemble of copious almost-equal-size light fragments. At reduced excitation, just sufficient for attaining the freeze-out, the break-up partition might evolve to more asymmetric configurations, where the formation of a heavy fragment close to the mass of the hot remnant is accompanied by one or more light fragments and clusters. As an extreme, this configuration might even reduce to a binary asymmetric decay. In the case of a very asymmetric split of the system, the partition multiplicity has minor influence on the kinematics of the light ejectiles. The emission of light particles populates spherical shells in velocity space and can not be easily distinguished by the kinematics from a binary decay when large mass-asymmetries characterize the partition. A bi-

nary or binary-like decay issued from a break-up configuration is a “fast” process. Compared to asymmetric fission, asymmetric break-up decays should result in a similar U-shape of the mass spectra of the yields. On the other hand, break-up decays should be reflected in the higher magnitude of the yields, and in the emission kinematics that, still mostly governed by the Coulomb field, should exhibit an additional contribution due to the eventual expansion of the source.

B. Measurement of light-fragment properties

Great part of the information on light-particle emission at high excitation energies was collected in 4π -type experiments, suited for measuring the multiplicity and the correlations of intermediate-mass fragments [38, 39, 40]. Still, the measurement of correlations and the linear-momentum-transfer was the basis for pursuing intense researches on the transition from the formation of compound nuclei to multifragmentation [41, 42].

In this work, we discuss additional results derived from new inclusive measurements of the reactions $^{56}\text{Fe}+p$ and $^{56}\text{Fe}+^{\text{nat}}\text{Ti}$ at 1 A GeV, effectuated in inverse kinematics with the FRagment Separator (FRS) [43] at GSI (Darmstadt). The experimental set-up was not intended to measure multiplicity and correlations, but to provide formation cross sections and high-resolution velocity spectra for isotopically identified projectile-like residues. The excitation of the $^{56}\text{Fe}+p$ system consists of purely thermal energy, and it is just high enough to approach the conditions for the onset of multifragmentation. On the basis of these data we search for the properties of the early appearance of break-up events and their competition with compound-nucleus emission. The system $^{56}\text{Fe}+^{\text{nat}}\text{Ti}$ is compatible with an abrasion picture. The excitation energy deposited in the projectile spectator, still mostly of thermal nature, establishes the dominance of multifragmentation in the decay process. We will especially discuss the differences in the kinematics of light-fragment emission in the two systems, conditioned by two different levels of excitation magnitude.

II. EXPERIMENT AND ANALYSIS PROCEDURE

The experiment was performed at GSI (Darmstadt). A primary beam of ^{56}Fe was delivered by the heavy-ion synchrotron SIS at an energy of 1 A GeV. The target was constituted of liquid hydrogen (with a thickness of 87.3 mg/cm^2) contained in a cryostat with thin titanium windows (36.3 mg/cm^2 in total), wrapped in thin Mylar foils ($\text{C}_5\text{H}_4\text{O}_2$, total thickness: 8.3 mg/cm^2) for thermal insulation. In the target area, other layers of matter intersected the ion-beam: the accelerator-vacuum window of titanium (4.5 mg/cm^2) and the beam-current monitor composed of aluminium foils (8.9 mg/cm^2). In or-

der to disentangle the production and the physical results related to the interaction with hydrogen from the contribution associated to the other materials, the whole experimental runs were repeated in identical conditions, after replacing the target by titanium foils having the same thickness of the cryostat windows and wrapped in Mylar foils having the same thickness of the cryostat insulation. This procedure did not only determine the disturbing contributions in the measurement of the $^{56}\text{Fe}+p$ system, but it also provided additional experimental data on an other reaction system. With some arbitrariness we name “titanium target ($^{\text{nat}}\text{Ti}$)” the ensemble of the titanium foils replacing the cryostat window, the Mylar wrapping, the accelerator-vacuum window and the beam-current monitor. Unfortunately, the measurement of the $^{56}\text{Fe}+^{\text{nat}}\text{Ti}$ system accounts also for non-titanium nuclei, the pollution of which corresponds to their portion in the total number of target nuclei per area and is equal to 25.9% (Al) + 7.2% (Mylar) = 33.1%. It should be remarked that these components are not placed at the same distance from the entrance of the spectrometer. Fragments produced in the beam-current monitor or in the accelerator-vacuum window could have lower probabilities to be registered in the experiment since the angular acceptance is reduced by factors of 0.33 and 0.25, respectively, compared to products from the titanium foils replacing the cryostat. Henceforth, we refer to the liquid hydrogen as “proton target (p)”. In this case no polluting contributions are included in the final results.

A. Nuclide identification

The reaction products were analysed with the high-resolution magnetic spectrometer FRS, constituted of four dipoles set in an achromatic mode. The horizontal positions of the reaction products were deduced from two plastic scintillators, the first positioned in a dispersive plane after the first two dipoles, the second installed in the final achromatic plane. From the time of flight (TOF), evaluated between the two scintillators, the relative velocity β and the γ -factor were obtained. The particle charge q was measured with an ionisation chamber placed in front of the achromatic plane. Since the reaction products were fully stripped, the nuclear charge $Z = q$ was deduced directly. The mass A was deduced from the time of flight and the magnetic rigidity of the particles according to the relation

$$\frac{A}{Z} = \frac{1}{c} \cdot \frac{e}{m_0 + \delta m} \cdot \frac{B\rho}{\beta\gamma(TOF)}, \quad (1)$$

where $B\rho$ is the magnetic rigidity of a particle, c the velocity of light, e the elementary charge, m_0 the nuclear mass unit, $\delta m = dM/A$ the mass excess per nucleon. For the purpose of the isotopic identification, the variation of δm with A/Z can be neglected, and a linear variation of A/Z as a function of $B\rho/\beta\gamma$ can be assumed. In fig. 2, the raw data collecting all the events measured in the

experiment are shown. Events are ordered according to the measured Z and A/Z so as to obtain an isotopic identification plot.

B. Longitudinal velocities

The measurement of the time of flight is precise enough for an accurate identification of the mass of the fragments. Nevertheless, mainly due to the resolution and additionally due to a slight dependence on the trajectory [44] it is not suited for a fine measurement of the velocities of the fragments. On the other hand, once an isotope is identified in mass and charge, a much more precise measurement of the velocity is obtained directly from the magnetic rigidity of the particle

$$\beta\gamma = B\rho \cdot \frac{1}{c} \cdot \frac{e}{m_0 + \delta m} \cdot \frac{Z}{A}. \quad (2)$$

In this case, the precision of $\beta\gamma$ depends only on $B\rho$, that has a relative uncertainty of $5 \cdot 10^{-4}$ (FWHM) for individual reaction products. The absolute calibration of the deflection in the magnet in terms of magnetic rigidity $B\rho$ is performed at the beginning of the experiment with a dedicated calibration run using the primary beam.

Since one single magnetic configuration of the FRS selects only a $B\rho$ range of about $\pm 1.5\%$, several overlapping runs have been repeated imposing different magnetic fields. While for the heavy residues close to the

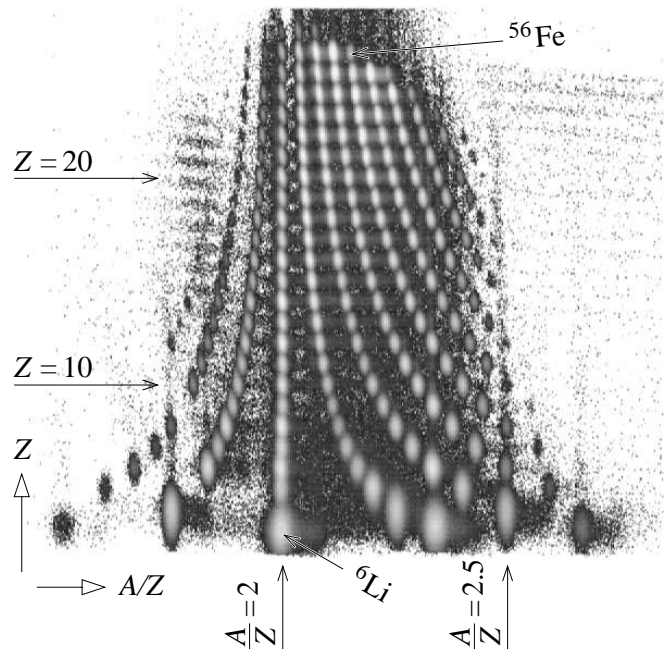


FIG. 2: Experimental isotopic resolution. The isotopes are grouped in chains. One chain collects nuclei having the same value of the difference $N - Z$. The straight chain corresponds to $A/Z = 2$ or $N - Z = 0$. On the right of this chain the isotopes are neutron rich, on the left they are proton rich.

projectile one or few settings were sufficient to cover the whole velocity spectrum, the light fragments often required more than ten runs. The $B\rho$ scanning of ${}^6\text{Li}$, produced in the interaction with the target of liquid hydrogen enclosed in the cryostat constitutes the diagram (a) of fig. 3: each segment of the spectrum is obtained from a different scaling of the set of magnetic fields of the FRS. In order to obtain consistent weightings, the counts of the different measurements were normalized to the same beam dose. For each magnetic scaling, this normalization was obtained by dividing the corresponding segment of the spectrum by the number of projectiles that hit the target during the corresponding run. The impinging projectiles were counted with the beam-current monitor. The renormalized yields are shown in the diagram (b) of fig. 3. We should note that the spectrometer accepts only the fragments emitted in a cone of about 15 mr around the beam-axis in the laboratory frame, when the reaction occurs in the hydrogen-target position. As a consequence, a light residue like, for example, ${}^6\text{Li}$, generated in a collision at a beam energy of 1 A GeV can be detected only if emitted with small transverse momentum. The experimental spectrum represents the part of the density distribution in the velocity space selected by the angular acceptance of the spectrometer, projected on the longitudinal axis. Unfortunately, the angular acceptance depends on the magnetic rigidity of the particles. As pointed out in the work [45], for a given set-up of the spectrometer, the more the intersection of the trajectory of a particle with the dispersive or the achromatic planes is displaced from the centers, the lower is the acceptance angle of the FRS. The effect appears in the curved sides of each single segment, with the result of disturbing the overall structure of the $B\rho$ scanning. This distortion, seen in the spectrum of the plot (b) of fig. 3, can be successfully corrected by means of ion-optical calculations that fix the dependence of the angular transmission on the trajectory. The calculation of the ratio of the transmission T relative to its maximum value is presented in fig. 4. The corrected spectrum, seen in the plot (c) of fig. 3, is the result of scaling up the yields of the spectrum by the factor T_{max}/T . We also changed from a $\beta\gamma$ spectrum to a longitudinal-velocity spectrum and, to simplify the analysis, the reference frame was changed from the laboratory to the beam frame. On the average, the projectile interacts in the middle of the target.

Therefore, we take into account the slowing down of ${}^{56}\text{Fe}$ in the first half of the target, as represented in the upper diagram of fig. 5. We also consider that the fragments slowed down in the remaining half of the target and, therefore, were emitted at higher velocity than the one we observed. The analysis so far illustrated was repeated for all the isotopes produced in the interaction with the target of liquid hydrogen enclosed in the cryostat. Successively, the same procedure was applied to the corresponding isotopes produced in the interaction with the ${}^{\text{nat}}\text{Ti}$ target. As all spectra are normalized to the same beam dose, by subtracting the velocity spectra

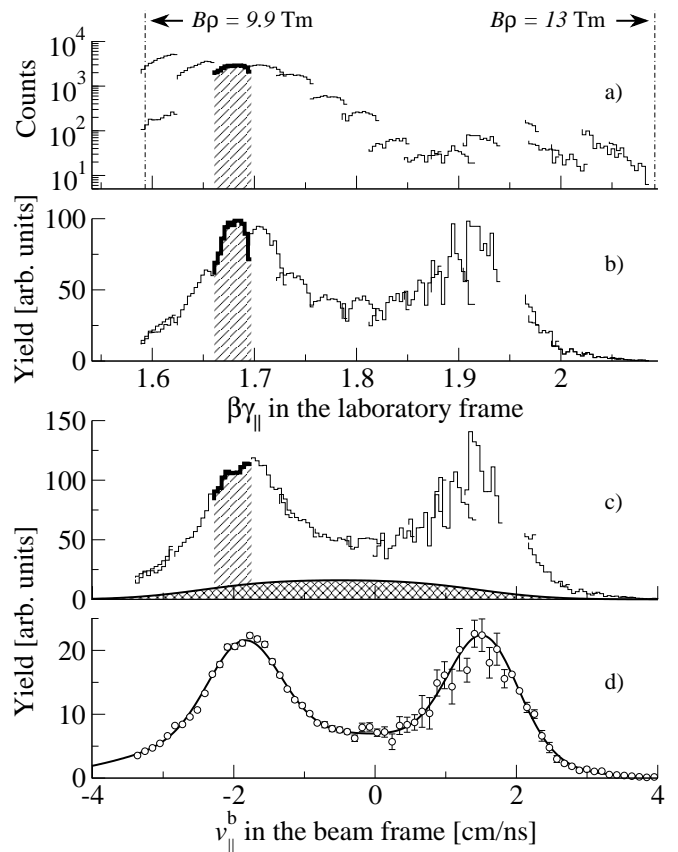


FIG. 3: Four steps of the analysis procedure to obtain the observed velocity spectrum of ${}^6\text{Li}$ emitted in the reaction ${}^{56}\text{Fe}+p$. (a) Raw spectra of counts as a function of $\beta\gamma$ in the laboratory frame. Each segment results from a different scaling of the magnetic fields of the FRS. One segment associated to the same magnetic scaling is marked with hatched areas in this plot and in the two following ones. Arrows delimit the scanned $\beta\gamma$ range. (b) Yields normalized to the same beam dose. (c) Elimination of the angular-transmission distortion. Spectrum as a function of the longitudinal velocity in the beam frame v_{\parallel}^b . The broad Gaussian-like hatched area indicates the contributions from non-hydrogen nuclei. (d) All components of the spectrum are composed together averaging overlapping points. Contributions from non-hydrogen-nuclei were suppressed. The spectrum was divided by the number of nuclei per area of the liquid-hydrogen target. Statistical uncertainties and a fit to the data are shown.

of the residues produced in ${}^{56}\text{Fe}+{}^{\text{nat}}\text{Ti}$ (indicated by the hatched area in the plot (c) of fig. 3) from those of the corresponding isotopes produced in the target of hydrogen stored in the cryostat, we could obtain the measured velocity distributions for the reaction with the liquid hydrogen. The resulting yields are unambiguously disentangled from any disturbing contributions produced by other material present in the target area. Finally, the velocity spectra obtained for the ${}^{56}\text{Fe}+p$ system were divided by the number of nuclei per area of the proton target. The resulting spectrum is shown in the diagram (d) of fig. 3.

In the case of the $^{56}\text{Fe} + \text{natTi}$ system, we should consider that the target is constituted of three components, the titanium foils replacing the cryostat, the beam-current monitor and the accelerator-vacuum window, having a number of nuclei per area equal to n_0 , n_1 , and n_2 , respectively. We should also recall that these components are placed at different distances from the entrance of the spectrometer and are subjected to different values of the angular acceptance, that is about $\alpha_0 = 15.8$ mr, $\alpha_1 = 9$ mr, and $\alpha_2 = 7.8$ mr, for the layers n_0 , n_1 , and n_2 , respectively. Thus, the cross sections given in this work for the "titanium" target are calculated using a target composition where the different layers are weighted by the corresponding estimated transmission values T , assuming identical production cross sections in the different target components. In particular, the velocity spectra obtained for the $^{56}\text{Fe} + \text{natTi}$ system should be divided by the quantity $n_0T(\alpha_0) + n_1T(\alpha_1) + n_2T(\alpha_2)$.

The experimental data are already complete enough to let us recognise an important signature of the Coulomb repulsion: the double-humped spectrum reveals that the velocity of ^6Li nuclei emitted at small angles has two components: one appreciably higher and one appreciably lower than the beam. According to the references [46, 47, 48], where similar structures have been observed for fission fragments, we may connect the double-humped spectrum to the action of the Coulomb field of a heavy partner in the emission process.

Once changed to longitudinal velocities in the beam-frame v_{\parallel}^b , the shift of the barycenter of the spectrum with respect to zero is equal to the mean reaction recoil $\langle v_{\parallel}^b \rangle$. Also this quantity, studied in the lower diagram of fig. 5, carries a valuable information about the reaction mechanism, and it can be related to the friction suffered by the projectile in the collision, according to a given impact parameter [49]. Due to the limited angular acceptance of the FRS which favours the detection of heavier nuclei, a depletion of the statistics for the measurement of the lightest nuclei is expected when, as in this case, the light fragments are measured together with the heaviest in the same magnetic setting. Due to these

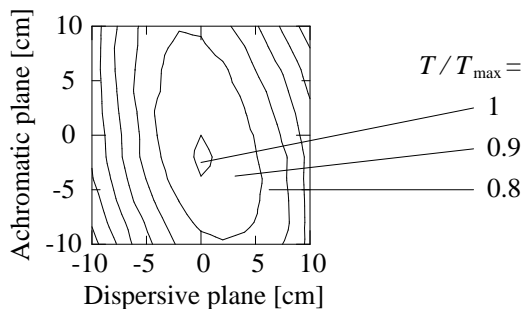


FIG. 4: Transmission of the FRS as a function of the positions in the dispersive and achromatic planes, relative to its maximum value. Numerical values are taken from ref. [45].

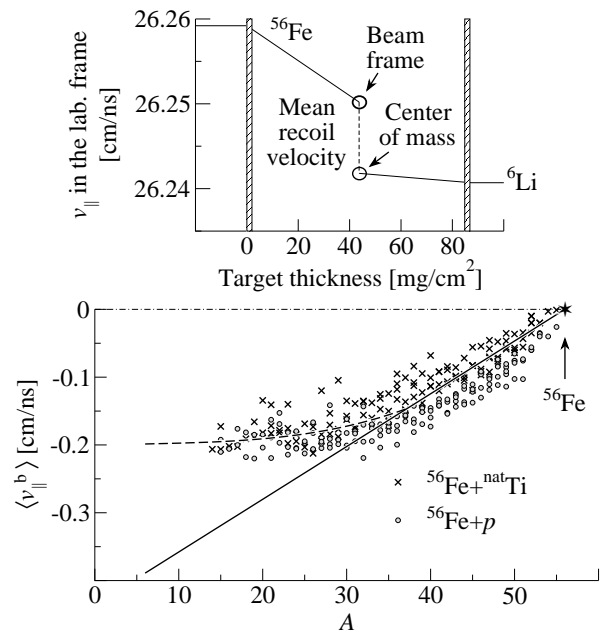


FIG. 5: *Top.* Definition of the beam frame and of the center-of-mass frame of the emitting source with respect to the laboratory frame. The diagram corresponds to realistic conditions of the present experiment for ^6Li . The solid lines describe the slowing down of the beam and of the centroid of the velocity spectrum of ^6Li in traversing the target. *Bottom.* Mean longitudinal recoil velocities in the beam frame $\langle v_{\parallel}^b \rangle$ of the reaction residues compared with the systematics of Morrissey [49] (solid line); only isotopes with sufficient statistics and entirely measured velocity spectra are considered.

problems, the mean velocities of the light residues can only be determined with relatively large uncertainties. With these large uncertainties, the information from the mean velocities could not be exploited. Although these mean velocities also enter into the evaluation of the cross sections, the uncertainties they introduce are comparable to those from other sources. We preferred to deduce the mean recoil velocities of lithium, beryllium, boron and carbon by extrapolation from the systematics of the data relative to the ensemble of the heavier residues.

III. RESULTS

A. Nuclide cross sections

When a fragment is emitted with a large absolute velocity $v = |\vec{v}|$ in the center of mass, not all the angles of the corresponding velocity vector \vec{v} are selected by the finite angular acceptance of the spectrometer. As a result of the data analysis detailed in the previous section, we obtain the measurement of the apparent cross section $d\mathcal{I}(v_{\parallel})/dv_{\parallel}$ as a function of the longitudinal velocity v_{\parallel} . This observed cross section differs from the real cross section due to the angular acceptance. The detec-

tion of a particle depends on the perpendicular velocity $v_{\perp} = \sqrt{v^2 - v_{\parallel}^2}$ in the center-of-mass frame, the angle of rotation around the beam direction φ , and the velocity u of the center of mass with respect to the laboratory. The dependence on φ comes about because the beam pipe inside the quadrupoles is not cylindrical. To reconstruct the full velocity distribution, independent of the angular acceptance of the spectrometer, an assumption on the angular distribution is necessary. It was concluded from experiments, to which the full angular range was accessible, that the data are in satisfactory agreement with an isotropic emission (see, for example, the treatment of “Moving source analysis” presented in [50]). This assumption has been corroborated by a vast collection of data for reactions of very different nature. Isotropic emission has been observed either for lowly excited fissioning systems [6], or even for very highly excited nuclei undergoing expansive flow in thermal multifragmentation [16, 17]. At least the $^{56}\text{Fe}+p$ system can be safely included in this range. Slightly less justified is the assumption for $^{56}\text{Fe}+^{\text{nat}}\text{Ti}$, since some effects of dynamical multifragmentation could disturb the isotropy.

Thus, if we assume isotropic particle emission in the center-of-mass frame, the variation of the cross section $\sigma(v)$, as a function of the absolute velocity v , is related

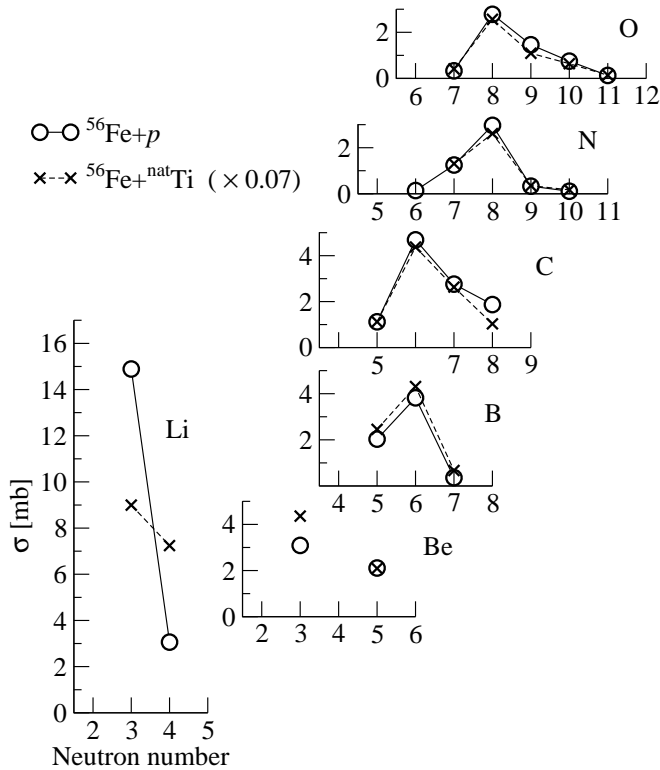


FIG. 6: Experimental isotopic production cross sections of some light elements for the reactions $^{56}\text{Fe}+p$ and $^{56}\text{Fe}+^{\text{nat}}\text{Ti}$ at 1 A GeV. The cross sections related to the latter system are scaled of a factor 0.07. Numerical values are collected in table I.

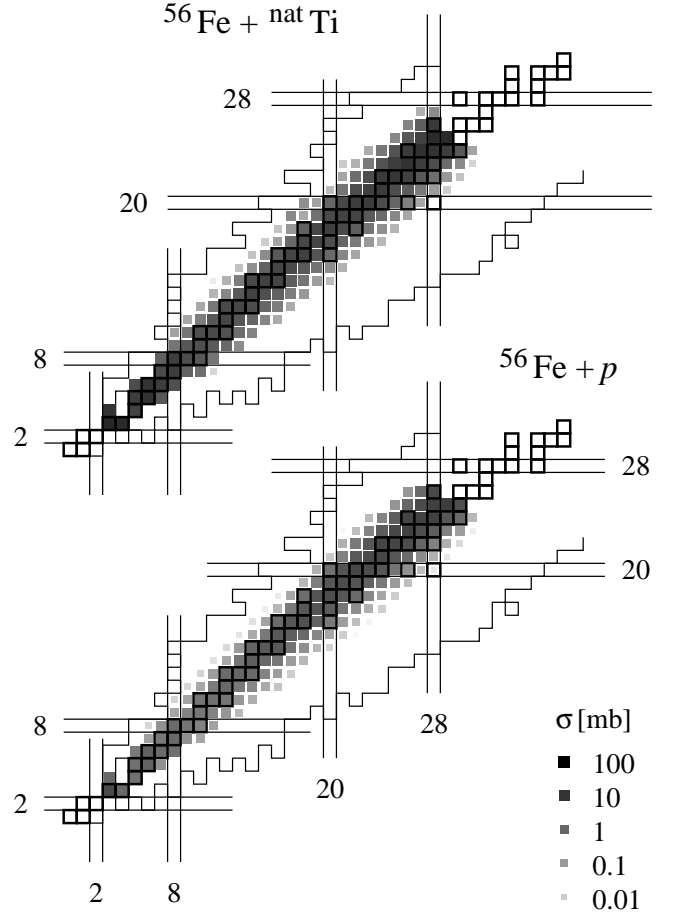


FIG. 7: Isotopic production cross sections shown on a chart of the nuclides for the reactions $^{56}\text{Fe}+p$ and $^{56}\text{Fe}+^{\text{nat}}\text{Ti}$ at 1 A GeV. The values for ^{54}Mn in $^{56}\text{Fe}+p$ and for ^{53}Cr in $^{56}\text{Fe}+^{\text{nat}}\text{Ti}$ were obtained from systematics.

to the variation of the apparent cross section $\mathcal{I}(v_{\parallel})$ as a function of v_{\parallel} by the equation (see appendix A 1):

$$\frac{d\mathcal{I}(v_{\parallel})}{dv_{\parallel}} = \frac{1}{4\pi} \int_0^{2\pi} d\varphi \int_{|v_{\parallel}|}^{\sqrt{v_{\parallel}^2 + \tilde{v}_{\perp}^2(\varphi)}} \frac{1}{v} \frac{d\sigma(v)}{dv} dv \quad , \quad (3)$$

where $\tilde{v}_{\perp} = \tilde{v}_{\perp}(\varphi, u)$ is the highest value of v_{\perp} selected by the angular acceptance of the spectrometer, and φ is the rotation angle around the beam direction. As demonstrated in the appendix A 2, it is possible to reverse the relation (3) and extract $d\sigma(v)/dv$ by the straightforward solution of a system of geometric relations. The formation cross sections are directly obtained by integration of $d\sigma(v)/dv$. In the appendix B, table I collects the isotopic cross sections for the production of light residues, from lithium up to oxygen, measured in this work for the reaction $^{56}\text{Fe}+p$ and $^{56}\text{Fe}+^{\text{nat}}\text{Ti}$. The distributions of the formation cross sections evaluated for the two systems $^{56}\text{Fe}+p$ and $^{56}\text{Fe}+^{\text{nat}}\text{Ti}$ at 1 A GeV are presented in fig. 6 for different elements as a function of the neutron number and in fig. 7, on the chart of the nuclides. The extension

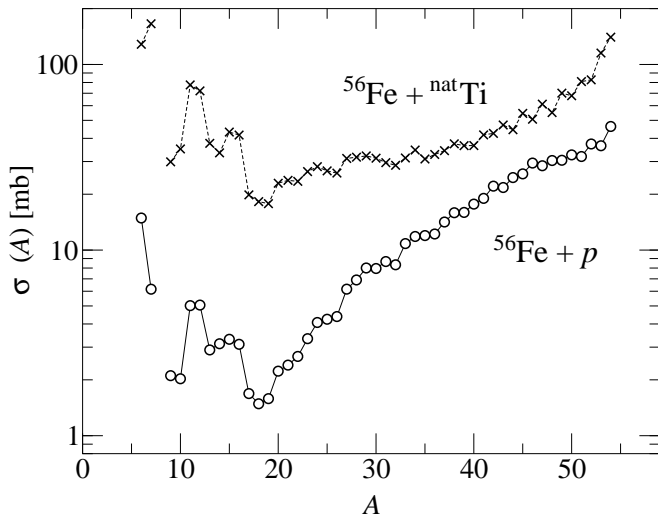


FIG. 8: Experimental production cross sections as a function of the mass number. The statistical uncertainties are lower than 10%. The systematic uncertainties evolve from 10% for the heavy residues close to the projectile to 20% for the light fragments.

of the production appears rather similar and, in particular, despite the expected difference in excitation energy reachable in the collisions with the two different targets, the cross-section distributions of the residues of the two reactions do not manifest drastic differences in their features. A more quantitative revelation of this similarity is presented in fig. 8, where the mass distributions are compared. The difference in the shape of the mass spectra is significant only for the intermediate masses: the cross section of the residues of $^{56}\text{Fe}+p$ decreases from $A = 30$ to $A = 18$ by about one order of magnitude, while we observe only a slight decrease by about a factor of two for $^{56}\text{Fe}+^{\text{nat}}\text{Ti}$. The data reveal that higher excitation energy introduced by the interaction with titanium, with respect to proton-induced spallation, results in decreasing the slope of the mass-spectra in the IMF-range and depleting the cross section for heavy residues in favour of an enhanced production of light fragments. However, the portion of the mass spectra corresponding to light-particle emission follows a very similar exponential slope for both systems.

B. Velocities

In the previous section, the full velocity distributions were reconstructed from the data and employed to obtain the residue formation cross sections for the reactions induced by the proton and titanium target, respectively. Though, the cross sections did not yield any unambiguous distinction between the two reactions that, indeed, should result into rather different deexcitation pictures on the basis of the different thermal excitations reached

in the two systems. On the contrary, the particularity of the proton-induced spallation compared to the titanium-induced fragmentation arises strikingly when the kinematics of the light-particle emission is investigated. The density of velocity vectors \vec{v} in a plane containing the beam axis is presented in fig. 9. (As observed in the following, this presentation is equivalent to invariant-cross-section plots.) Thus, when we compare the $^{56}\text{Fe}+p$ system to the $^{56}\text{Fe}+^{\text{nat}}\text{Ti}$ system on the basis of the recoil velocity, we find that substantially distinct mechanisms should be involved in the light-fragment emission in the two systems. In the fragmentation reaction induced by the titanium target, all the residues are emitted according to a bell-shape velocity spectrum. A long sequential decay would produce this kind of shape; in this process, neutrons, protons and clusters are in fact emitted with different angles with equal probability. Nevertheless, due to the high excitation of the hot fragments gained in such a violent collision, and due the exponential increase of the cross section of the light residues with the mass loss, we are in favour of a multifragmentation picture to depict the dominant deexcitation process. In this

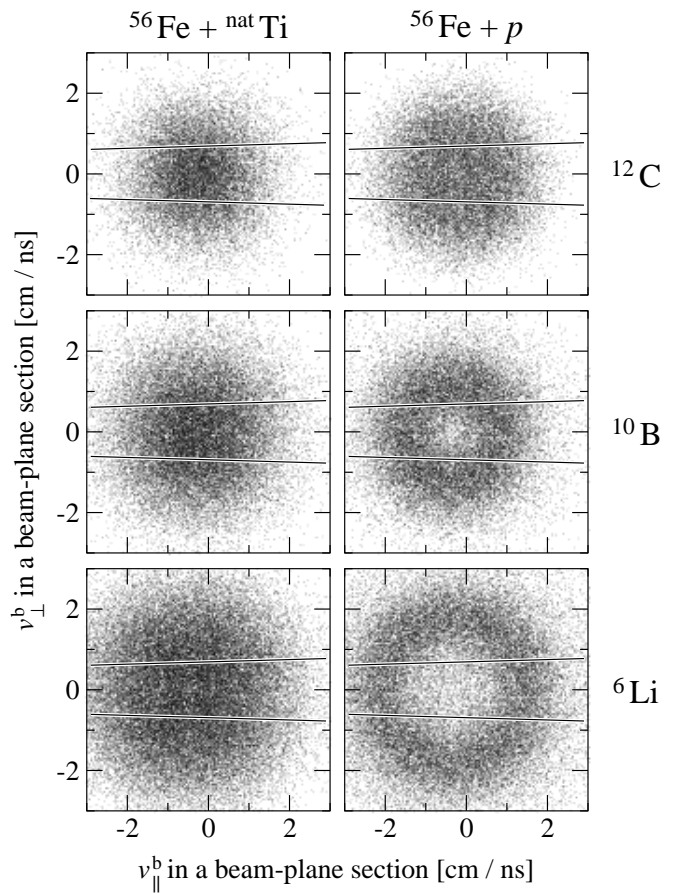


FIG. 9: Reconstructed density plots in velocity space in the beam frame $(v_{\parallel}^b, v_{\perp}^b)$ representing the distribution on a plane containing the beam axis. The solid lines denote the angular acceptance of the spectrometer.

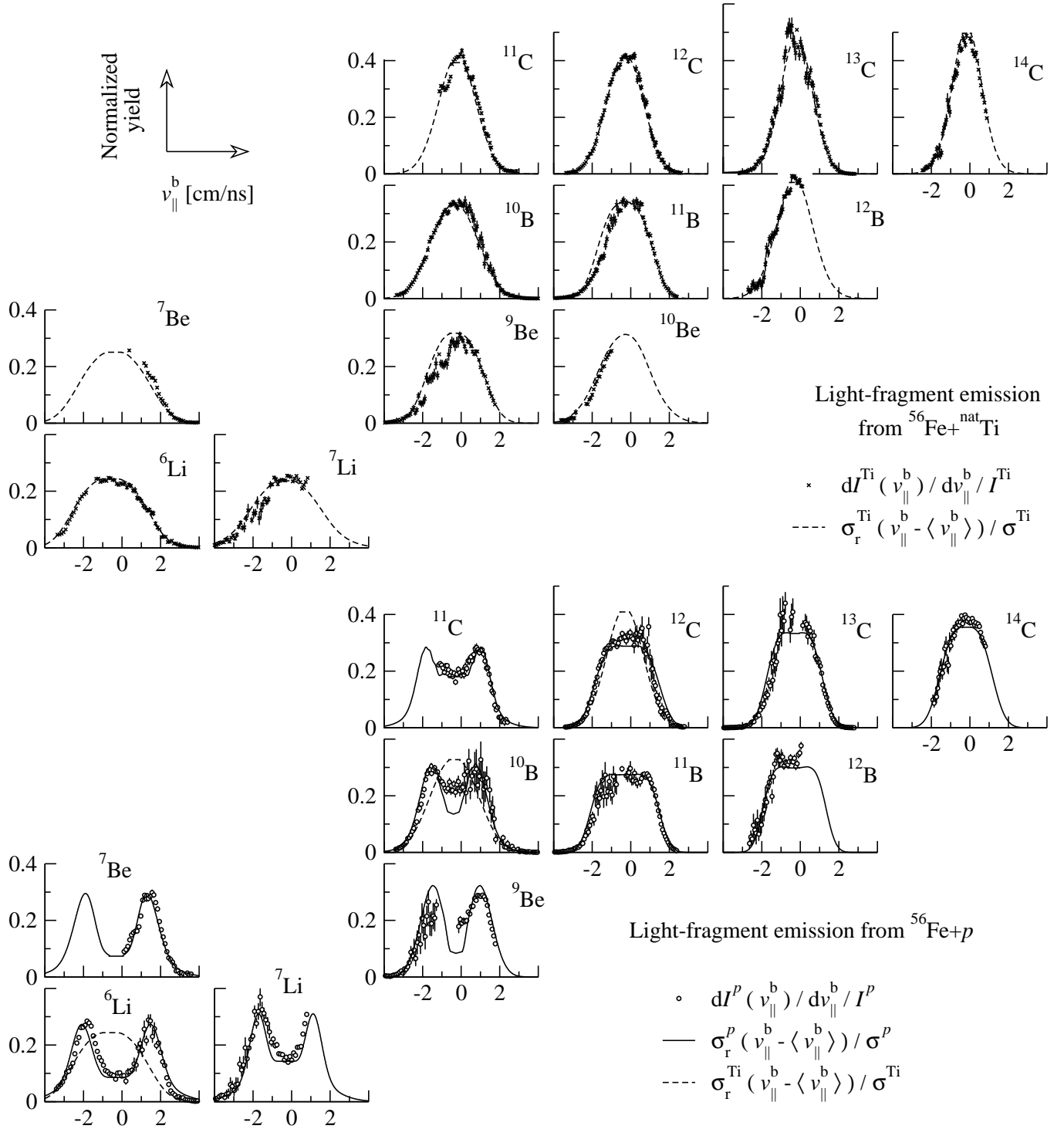


FIG. 10: Velocity spectra of light residues produced in $^{56}\text{Fe} + \text{natTi}$ (upper diagram), and in $^{56}\text{Fe} + p$ at 1 A GeV (lower diagram), ordered on a nuclear chart. They are represented as a function of the velocity in the beam direction in the beam frame v_{\parallel}^b . Crosses and points indicate measured spectra $dZ^{\text{Ti}}/dv_{\parallel}^b$ and dZ^p/dv_{\parallel}^b , respectively, defined according to eq. (3), and normalized to the unit. They represent all fragments transmitted through the FRS. Reconstructed velocity spectra σ_r^{Ti} and σ_r^p , defined according to eq. (4) and normalized to the unit are marked with dashed and solid lines, respectively. In the lower diagram, the reconstructed spectra for ^6Li , ^{10}B and ^{12}C emitted from $^{56}\text{Fe} + \text{natTi}$ are superimposed as dashed lines for comparison.

case, the hot source is expected to undergo a fast expansion and successively form several fragments. In this scenario [13], the emission velocity of a light residue could vary largely according to different parameters: the partitioning in the multifragmentation event, the expansion of the source before the break-up phase, and the position where the tracked fragment is formed with respect to the other fragments. Also this process would result in a velocity spectrum with a bell shape centered at the mean recoil velocity, equal to the shape we observe.

On the contrary, when light fragments originate from the $^{56}\text{Fe}+p$ system, the reaction dynamics leads to the population of one most probable emission shell in the velocity space, around the center of mass. This is the case of ^6Li , as shown in fig. 9. Only a forward and a backward portion of the emission shell could be measured as selected by the conical cut that the spectrometer determined: this fully explains the double-humped velocity spectra shown in fig. 3.

The velocity distributions of the light fragments generated in the proton-induced reaction carry the unambiguous signature of a strong Coulomb repulsion in the emission process. This observation evidently excludes that the light fragments could be the final residues of a long sequential evaporation chain. The strong Coulomb component in the emission process rather reflects the dominating influence of a very asymmetric split of the source.

We can now reduce the representation of the recoil-velocity distribution $\sigma(v)$ to one dimension, selecting only those velocities \vec{v} aligned in the beam direction, and occupying only abscissae in the plots of fig. 9.

Due to our assumption of isotropy, we can define radial velocity distributions dividing the differential cross section $d\sigma(v)/dv$ associated to a given velocity v in the center of mass by the spherical surface of radius v :

$$\sigma_r(v) = \frac{d^3\sigma}{d\vec{v}} = \frac{1}{4\pi v^2} \frac{d\sigma}{dv} \quad , \quad (4)$$

It should be remarked that either in the reference of the center of mass or in the projectile frame, γ is close to the unit and consequently $\sigma_r(v)$ is directly related to the invariant cross section $\sigma_I(v)$. Indicating $m = \gamma m$ the mass of the particle, $\vec{p} = \gamma \vec{p}$ its momentum and E its total energy in the center of mass frame (or in the projectile frame), we obtain the equality:

$$\sigma_r(v) = \frac{m^2 c^2}{m c^2} \frac{d^3\sigma}{d\vec{p}} = \frac{1}{c^2} E \frac{d^3\sigma}{d\vec{p}} = c^{-2} \sigma_I(v) \quad . \quad (5)$$

Also the planar cuts in velocity space ($v_{\parallel}^b, v_{\perp}^b$) of fig. 9 are equivalent to invariant-cross-section plots [51].

As a technical remark, the advantage of inverse kinematics compared to direct-kinematics experiments should be pointed out. The registration of emission velocities close to the velocity of the center of mass of the hot remnant are not prevented by any energy threshold. Thus, only in inverse kinematics we can clearly appreciate the gradual transition from a chaotic-dominated process,

reflected in Gaussian-like invariant-cross-section spectra, to a Coulomb- (or eventually expansion-) dominated process, producing a hollow around the center of mass. This characteristic signature we exploit resembles the investigation of relative velocity correlations between two fragments [52] in full-acceptance experiments for analysing decay times. In that case, the probability to detect two almost simultaneously emitted particles in space with small differences in direction is suppressed due to the mutual Coulomb interaction.

A systematic study of the spectra of lithium, beryllium, boron and carbon is presented in fig. 10 and compared with the observed velocity distributions. In the $^{56}\text{Fe}+^{\text{nat}}\text{Ti}$ reaction, all spectra show a bell shape. In the $^{56}\text{Fe}+p$ spallation, the double-humped distribution appears clearly for isotopes with mass lower than twelve units. The shape of the velocity spectra depends mostly on the mass rather than on the charge, and chains of isotopes belonging to the same elements show a transition from a bell shape toward a double-humped spectrum with decreasing mass. This transition is not always gradual but, as revealed by the neighbouring ^{11}C and ^{12}C in the lower panel of fig. 10, sometimes seems to be rather abrupt.

IV. DISCUSSION

A. Systematics of kinematical features

On the basis of the ensemble of experimental data on the production cross section and on the emission velocity of the residues, we devote this section to discuss the reaction phenomenology. In accordance to the vast literature dedicated to ion-ion fragmentation (explored in the reviews [13, 22]), we can safely relate the $^{56}\text{Fe}+^{\text{nat}}\text{Ti}$ reaction to the formation of highly excited systems, the decay of which is commonly interpreted as a multi-body instantaneous disassembly. In the following, we will refer to the $^{56}\text{Fe}+^{\text{nat}}\text{Ti}$ collision as a guideline for comparing to a fragmentation scenario. We will rather concentrate on the reaction mechanism of the proton-induced collision, which points to competitive types of decay at the same time.

From a first analysis, the main kinematical characteristics of the $^{56}\text{Fe}+p$ system, recalling a strong Coulomb repulsion, evocate a binary decay process.

On the other hand, other relevant features, like the high production yields for both light and about half-projectile-mass residues, could evocate the character of a fast decay, in line with the scenario of a sudden disassembly of the source depicted for the $^{56}\text{Fe}+^{\text{nat}}\text{Ti}$ system.

Our first attempt will be to test the pertinence of the experimental data on the emission velocities with a general systematics. Afterwards, we will discuss the intricacy of the several possible contributions to the spectral shape of the kinetic-energy distributions, and the

difficulty to extract insight on the excitation energies involved in the reaction directly from the measurement.

1. Absolute-velocity spectra

A recurrent analysis of the Coulomb-repulsion aspects is the comparison of the distribution of absolute velocities of outgoing fragments $v = |\vec{v}|$ (where \vec{v} is the corresponding velocity vector in the center of mass of the hot remnant) with the systematics of total kinetic energy released in fission. We intend to follow this approach (e.g. [53]) to test the compatibility of the light-fragment emission in $^{56}\text{Fe}+p$ with an asymmetric-fission picture. The FRagment Separator is particularly efficient in measuring recoil velocities, because the magnetic rigidity of the residues is known with high precision (see section II B). Indeed, the identity of the mother-nuclei is hidden in the complexity of the interaction processes related to high-energy collisions, like the intra-nuclear cascade and some evaporation events prior to the binary decay. The present new data are especially significant as they are the first measurement of the velocities of fragments issued of proton-induced splits of iron-like nuclei. On the other hand, fission velocities of residues of light

nuclei have been widely investigated in fusion-fission experiments [4], with the advantage of excluding most of the ambiguities on the identification of the fissioning nucleus. Data on symmetric fission of nuclei close to iron, formed in fusion reactions were published by Grotowski et al. [54] and where the basis for the revised kinetic-energy-release systematics of Viola [55]. This systematics establishes a linear dependence of the most probable total kinetic energy E_k^t released in a symmetric fission to the quantity $Z^2/A^{1/3}$, evaluated for the mother nucleus:

$$E_k^t = aZ^2/A^{1/3} + b \quad , \quad (6)$$

where A and Z identify the fissioning nucleus and a and b are parameters fitted to the experimental data ($a = (0.1189 \pm 0.0011)$ MeV, $b = (7.3 \pm 1.5)$ MeV). More recently, new data obtained for the binary split of even lighter nuclei than iron inspired Tavares and Terranova [56] to revisit the systematics of Viola once more. The new systematics is close to the systematics of Viola for heavy nuclei down to $Z^2/A^{1/3} \approx 200$. As shown in the insert of fig. 11, iron-like nuclei constitute a turning point: for lower masses the function changes slope, so that the total kinetic energy released vanishes for Z approaching 0. As anticipated by Viola [55], the expectation for a slope change around iron results by the effect of diffuseness of light nuclei in disturbing the formation of the neck, in the liquid-drop picture. The following relation was deduced:

$$E_k^t = \frac{Z^2}{aA^{1/3} + bA^{-1/3} + cA^{-1}} \quad , \quad (7)$$

where a , b and c are fitting parameters ($a = 9.39\text{MeV}^{-1}$, $b = -58.6\text{MeV}^{-1}$, $c = 226\text{MeV}^{-1}$).

Since the systematics is valid for symmetric splits only, a term should be added to extrapolate to asymmetric splits, when two fragments are formed with masses m_1, m_2 , mass numbers A_1, A_2 , and charges Z_1, Z_2 , respectively. Following the hypothesis of non-deformed spheres at contact (as also imposed in [56]), the Coulomb potential is proportional to the product of the charges of the fission fragments $Z_1 Z_2$, divided by the distance of their centers, which varies with $A_1^{-1/3} + A_2^{-1/3}$. The conversion from the symmetric to asymmetric configuration is therefore :

$$\frac{E_k^t}{E_{k,\text{symm}}^t} = \frac{Z_1 Z_2 / (A_1^{1/3} + A_2^{1/3})}{\left(\frac{Z}{2}\right)^2 / \left[2\left(\frac{A}{2}\right)^{1/3}\right]} \quad . \quad (8)$$

It should be remarked that the possible presence of a neck is not included in this simple relation that, therefore, is a good approximation for light systems only. From the momentum conservation and the introduction of the reduced mass $\mu = m_1 m_2 / (m_1 + m_2)$, we can relate the total kinetic energy to the velocity v_1 of the fragment A_1

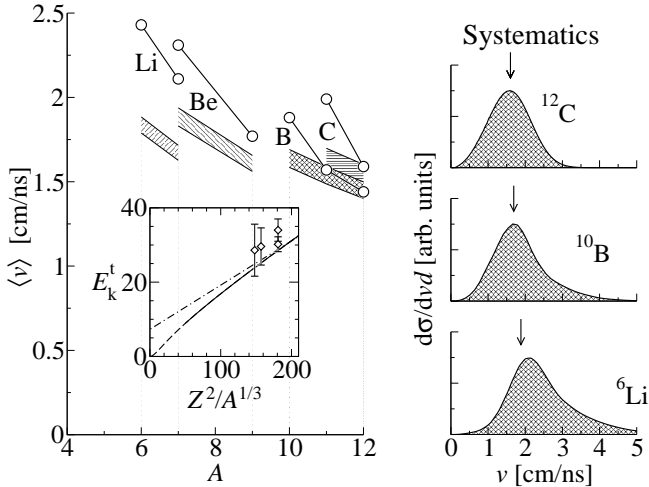


FIG. 11: *Left panel* Mean absolute velocities in the reference frame of the center of mass of the hot remnant, measured for residues of the $^{56}\text{Fe}+p$ system (open circles) and deduced from the systematics of Tavares and Terranova [56] (hatched bands). The width of the hatched areas results from the range of the possible mother nucleus from ^{46}Ti (lower values) to ^{56}Fe (higher values). In the insert, data points on the total kinetic energy released in a symmetric split of nuclei close to iron, measured by Grotowski et al. [54] are compared to the systematics of Viola [55] (dot-dashed line) and with the systematics of Tavares and Terranova [56] (solid line). *Right panel* Measured absolute-velocity spectra for the residues ^6Li , ^{10}B , and ^{12}C produced in the $^{56}\text{Fe}+p$ system. The arrows indicate the values obtained by the systematics of Tavares and Terranova.

by the relation $E_k^t = m_1^2 v_1^2 / 2\mu$. Introducing the latter form of E_k^t in the relations (8), and substituting the total kinetic energy released in symmetric fission with the corresponding value given by the systematics E_{syst}^t , we obtain the conversion

$$\frac{v_1^2}{E_{\text{syst}}^t} = 2^{11/3} \frac{\mu}{m_1^2} \frac{A^{1/3}}{A_1^{1/3} + A_2^{1/3}} \frac{Z_1 Z_2}{Z^2} . \quad (9)$$

Following the strategy of previous publications, e.g. [53], for the same light residues we compare the centroids of the measured absolute velocity spectra to the predicted velocities in fission events; the latter are deduced from the systematics of total kinetic energy released in fission by applying the relation (9). In the right side of fig. 11 we observe that, while the most probable absolute velocity does not diverge considerably from the systematics (assumed for ^{56}Fe as mother nuclei), the spectra of lighter fragments exhibit a long exponential tail for very high velocities. As a consequence of the asymmetry of the absolute velocity spectra with respect to a Gaussian distribution, the experimental centroids lie above the fission systematics, as shown in the left side of fig. 11. The hatched bands represent the range in velocity due to an assumed variation of the mother nucleus from ^{46}Ti (lower velocities) up to the projectile (higher velocities). In previous works (e.g. [16, 53, 57]) such tails to very high velocities, reflected in the divergence from the systematics, were related to the emission from an expanding system in its initial expansion stage.

2. Kinetic-energy spectra

Directly obtained from the absolute-velocity spectra, the distributions of kinetic energy E_k offer another representation of the kinematics, where some more classic

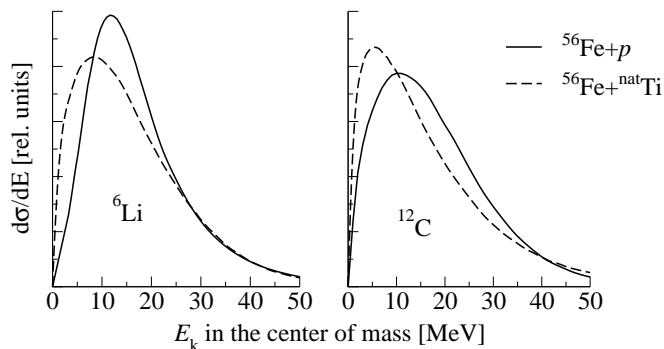


FIG. 12: Kinetic-energy spectra in the center of mass of the emitting source obtained from the reconstructed experimental velocity distributions in the case of emission of ^6Li and ^{12}C , respectively. The spectra are compared for the $^{56}\text{Fe}+p$ system (solid lines) and for the $^{56}\text{Fe}+\text{natTi}$ system (dashed lines). All spectra are normalized to the same area. The smooth distributions result from a spline fit procedure to the data.

features could be searched for. In fig. 12 similarities and differences in kinetic-energy spectra associated with proton and titanium target nuclei are illustrated. The tails to high emission velocities (fig. 11, right panel) lead to long tails in the kinetic-energy spectra and characterize both systems. We interpret it as a general indication that the collision generated very high excitation energy in the system. It would be tempting to even deduce the thermal properties of the system. In this case, with particular concern for the $^{56}\text{Fe}+p$ system, we could draw assumptions on the probability for break-up channels. Unfortunately, even if in some studies the nuclear temperature was deduced from the inverse slope parameter [20], the mixing up of several effects in the observed kinematics yields serious ambiguities in the extraction of thermal properties of the source. We can list at least eight of the combined effects describing the observed spectral shapes.

1. The presence of a Coulomb barrier results in the deviation of the spectral shape from a Maxwell-Boltzman distribution (the maximum moves to higher values).
2. The transmission through the barrier is ruled by a Fermi function with an inflection point at the barrier and not by a discontinuous step function. This effect introduces a widening of the spectrum.
3. As a result of the initial stage of the collision, an ensemble of several possible sources with different Z and A are related to different Coulomb barriers. The folding of different Coulomb barrier peaks results in a broader hump.
4. If emitted nuclei undergo further evaporation events, the spectrum widens.
5. The temperature of the hot source acts on the recoil momenta of the emitted fragments. If at least major disturbing effects like the variation of the emitting source, the Fermi momentum in the hot fragmenting nucleus, described below, and the transmission through the barrier were negligible, it would be possible to deduce the temperature of the equilibrated fragmenting system from the inverse slope parameter fitted to the tail of the high side of the energy spectrum of the residues.
6. The Fermi momentum of particles removed in the collision with protons or abraded in the interaction with the titanium target produces a momentum spread that could be evaluated according to Goldhaber's formalism [58].

$$\sigma_{p_F}^2 = \sigma_F^2 \frac{A_i(A - A_i)}{A - 1} , \quad (10)$$

where A is the mass of the hot remnant, A_i is the mass of the emitted cluster and σ_F is the Fermi-momentum spread. The momentum spread deriving from the Fermi-momentum spread produces a

distribution of momenta of the center of mass of the remnants in the projectile frame. In deducing the energy spectra of the residues in the frame of the center of mass of the remnant, the spread related to the Fermi-momentum could not be eliminated as the mass of the remnants are unknown. As a result, the Fermi-momentum contributes both to widening the spectrum and incrementing the tail for high energies. Quoting from Goldhaber [58], when a thermalised system with a temperature T and mass A emits a cluster of mass A_i , the momentum spread of the fragment spectrum is

$$\sigma_p^2 = m_0 k T \frac{A_i(A - A_i)}{A}, \quad (11)$$

where m_0 is the nuclear mass unit and k is Boltzmann's constant. The momentum spread σ_{p_F} related to the Fermi momentum adds to the momentum spread induced by the reaction. This means that, just reversing the previous relation, the additional contribution to the temperature related to the Fermi momentum is equal to the apparent temperature

$$T_{p_F} = \frac{\sigma_{p_F}^2}{m_0 k} \frac{A}{A_i(A - A_i)}. \quad (12)$$

As it was remarked in early studies [59], the extraction of the nuclear temperature from the measured energy spectra of the residues is therefore a dangerous procedure (a recent discussion of the problem of the Fermi motion is presented in [60]).

7. Multifragmentation events could be accompanied by the expansion of the nuclear system. Nuclei emitted in the initial instant of the expansion would populate the high-energy tail of the spectrum. This is the case for very excited systems [61].
8. The multiplicity of intermediate-mass fragments simultaneously emitted might be reflected in the maxima. According to previous investigations [62], a drop in the maximum energy of the outgoing fragments in a simultaneous disintegration of the source indicates higher average multiplicity of intermediate-mass fragments: this is related to the larger number of participants in the redistribution of the kinetic energy.

The last of the enumerated contributions to the energy spectra is evident in fig. 12. In the proton-induced collision, the position of the maximum corresponds to larger kinetic energy than in the case of the titanium target. This might be related to higher multiplicity of intermediate-mass fragments for the $^{56}\text{Fe} + \text{natTi}$ system.

From the analysis of velocity and energy spectra we conclude that no clear evidence of the action of a fission barrier could be found. Either fission channels are not favoured, or other processes obscured them, like additional evaporation stages or the contribution of many

mother nuclei rather different in mass. The most relevant result is the manifestation of high-velocity tails, which we interpreted as possible indications of a preequilibrium expansion phase.

B. Nuclear-model calculations

We had some hints that very highly excited systems are formed even in the $^{56}\text{Fe} + p$ interaction, but we could not extract quantitative values directly from the experiment. We could not recognise the presence of a fission barrier, but a more complete analysis is required to exclude that solely compound-nucleus decays are sufficient to explain the light-fragment production. Thus, we wish to carry out a complete reconstruction of the whole reaction process and compare the ensemble of experimental results with the calculations.

Henceforth, we will restrict to the $^{56}\text{Fe} + p$ system. In particular, we will discuss two possible descriptions for the dominant process of light-fragment formation: either a series of fission-evaporation decays from a compound nucleus, or a fast break-up of a diluted highly excited system, in line with a multifragmentation scenario. To fix the initial conditions for the two decay models, we previously need to calculate mass, charge and excitation-energy distributions of hot remnants, as these quantities are not observable in the experiment.

1. Calculation of the excitation energy of the hot collision remnants

The initial non-equilibrium phase of the interaction $^{56}\text{Fe} + p$ was described in the framework of the intranuclear cascade-exciton model developed by Gudima, Mashnik and Toneev [63]. The model describes the interaction of an hadron or a nucleus traversing a heavy ion, considered as a finite open system, composed of two degenerate Fermi gases of neutrons and protons in a spherical potential well with diffuse surface. The interaction, pictured as a cascade of quasi-free nucleon-nucleon and pion-nucleon collisions, produces high-energy ejectiles, that leave the system, and low-energy particles that are trapped by the nuclear potential. As many holes as the number of intranuclear collisions are produced in the Fermi gas. The number of trapped particles and the number of holes (or excitons, without distinction) determines the excitation energy of the so-called "composite nucleus".

Hot remnants are often treated as equilibrated or partially equilibrated systems, both in the case of compound-nucleus formation and at a freeze-out state. Thus, an additional thermalization process might be necessary to describe the transition from the initial non-equilibrium phase of the collision to the equilibrium phase governing the decay. Following the hypothesis of the preequilibrium exciton model, the intranuclear cascade continues to develop through the composite nucleus by a sequence

of two-body exciton-exciton interactions, until equilibrium is attained. Two kinds of decay characterize the composite nucleus: either the transition to a more complicated exciton state, or the emission of particles into the continuum. While in Griffin's model [64] all decays are equiprobable, successive developments proposed more elaborate descriptions of the competition between decay modes. However, when the conditions of the interaction lead to multifragmentation, the evolution of the composite nucleus is more complicated, as the system is supposed to expand. In the course of the expansion process, an intense disordered exchange of charge, mass and energy among its constituents is expected. The density of nuclear matter evolves to a more dilute state, the freeze-out, at which breakup occurs. Sophisticated thermal-expansion models were specifically developed to describe this thermalization process [16, 21]. Nevertheless, in our calculation we were less specific and we adopted Blann's preequilibrium exciton model [65], independently of the deexcitation scenario.

In fig. 13 we present a calculation of the hot-fragment distribution generated in the intranuclear cascade with and without the inclusion of a preequilibrium stage, respectively. More quantitatively, in fig. 14 the projections of the distribution are shown as a function of the excitation-energy-to-mass ratio and mass. We observe

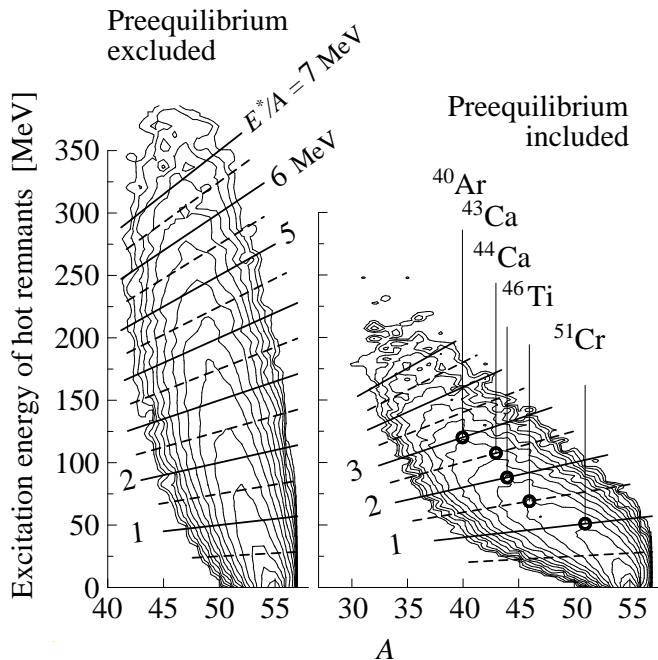


FIG. 13: Hot-fragment distributions generated in the intranuclear cascade [63], in the case of exclusion (left) and inclusion (right) of a preequilibrium stage [65], for the $^{56}\text{Fe}+p$ system. Straight lines define constant values of excitation energy per nucleon, indicated in MeV. Five selected isotopes correspond to the most probable mass and nuclear charge for a given excitation energy per nucleon.

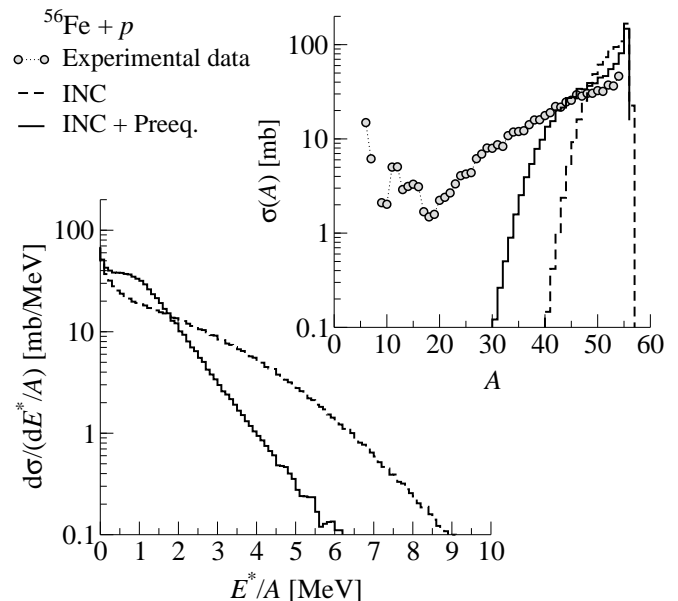


FIG. 14: Calculated production of the hot fragments after the intranuclear cascade (modelled according to [63]) and a preequilibrium stage (simulated according to [65]), for the $^{56}\text{Fe}+p$ system. The cross sections of the hot fragments are shown as a function of the excitation energy per nucleon E^*/A of the source (bottom-left) and the mass number (top-right). The mass distribution of cross sections of the hot fragments is compared to the experimental final-residue production.

that preequilibrium is particularly effective in evacuating part of the excitation energy and widening the distribution as a function of the mass. The hot-fragment mass distribution is compared to the measured production of the final residues, in order to indicate the extension of the deexcitation process.

When preequilibrium is suppressed, the energy per nucleon available for the deexcitation largely exceeds 2.5 MeV, a value that corresponds to the temperature of around 5 MeV, for a fully thermalised system. In this case, the multifragmentation regime is accessible. If preequilibrium is included, the average excitation of the system extends still right up to the expected threshold for a freeze-out state. Hence, according to this previous step of the calculation, oscillations in direction to breakup decays might be possible. Indeed, at these excitation energies break-up channels are expected to be still in competition with compound-nucleus decay. We will proceed to evaluate the extent of this competition by the use of deexcitation models.

2. Sequential fission-evaporation decay

In order to describe the deexcitation process in the framework of sequential fission-evaporation decays, we applied the code GEMINI [66]. Within GEMINI a spe-

cial treatment based on the Hauser-Feshbach formalism is dedicated to the emission of the lightest particles, from neutron and proton up to beryllium isotopes. The formation of heavier nuclei than beryllium is modelled according to the transition-state formalism developed by Moretto [5]. All asymmetric divisions of the decaying compound nuclei are considered in the calculation of the probability of successive binary-decay configurations. The total-kinetic-energy release in fission originally parameterised according to the systematics of Viola [55], eq. (6), was replaced by the systematics of Tavares and Terranova [56], formulated according to the relation (7), and extrapolated for asymmetric splits by the use of the conversion (9).

We simulated the decay of two possible ensembles of hot remnants, those issued directly from the stage of intranuclear cascade, and those which lost part of excitation energy and mass in a preequilibrium phase. The

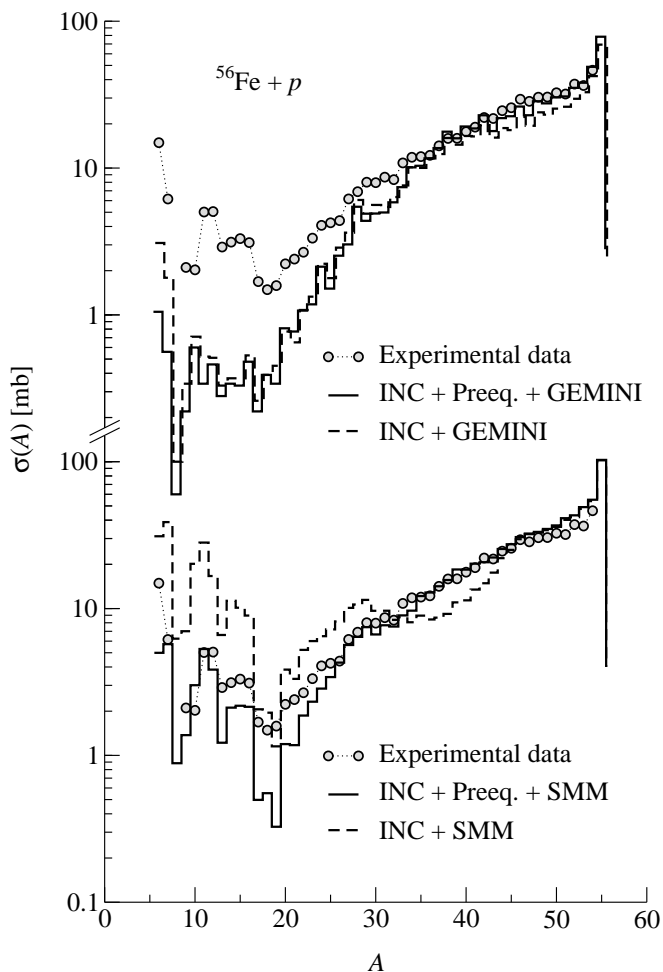


FIG. 15: Comparison of the measured mass distributions as a function of the mass number for the system $^{56}\text{Fe}+p$ with the results of GEMINI (upper part) and SMM (lower part). SMM is more sensitive than GEMINI to the effect of a preequilibrium phase.

resulting distributions of final residues are almost indistinguishable, revealing that the intermediate-mass fragments (especially those around oxygen) are not especially sensitive to the variation of average excitation energy of the system. It might be also pointed out that, when very hot fragments are allowed to decay by solely fission-evaporation channels, many nucleons and some light clusters are liberated at the very beginning of the deexcitation, before eventually forming an intermediate-mass fragment by fission. When the preequilibrium phase is suppressed, this preliminary emission could constitute a compensating process. In average, the relation between energy loss and mass loss could be similar in the two processes, and lead to analogous results. The difference is only conceptual, as the preequilibrium acts on a system still evolving toward thermalization, and particle evaporation is connected to a completely thermalised system. Only lithium and beryllium revealed a visible enhancement in the yields with the increase of average excitation energy.

The result of the model calculation, compared with the measured cross sections is presented in the upper side of fig. 15. The evaluation of the heavy-residue cross sections is consistent with the experimental data, but a sizeable underestimation of the production fails to reproduce the intermediate-mass region. Especially the production of the residues populating the characteristic hollow in the mass distribution reveals to be generally underestimated by the calculation. To complete the comparison, we turn now back to the first key observable found in our experimental investigation: the velocity spectra of light fragments. In the first row of fig. 16 the experimental spectra of ^6Li , ^{10}B , ^{11}C and ^{12}C are shown, together with their velocity reconstruction (solid line). Within GEMINI, all decays are decorrelated in time and when more fragments are produced they do not interact in the same Coulomb field. Binary compound-nucleus emission is connected with a restricted range of heavy sources close to the projectile mass, reflected in the small width of the Coulomb peaks, as shown in the second row of fig. 16. This feature characterizes only the formation of the lightest fragments and disappears with increasing mass of the residues. The calculations presented in the second row of fig. 16 should not be compared to the experimental data. The effect of the Coulomb repulsion involved in the deexcitation and disentangled from the smearing effect of the intra-nuclear cascade and preequilibrium emission can be appreciated in the third row of fig. 16, where the reference frame has been fixed to the center of mass of the initial system formed at the beginning of the fission-evaporation process. In the calculation, the transformation of the two Coulomb peaks into one single wide hump occurs for lower masses than experimentally observed. The model generates one single hump in the longitudinal velocity spectra of light fragments when a longer evaporation cascade is involved, and characterized by mainly alpha and nucleon emission. Moreover, the total width of the calculated spectra is narrower than observed.

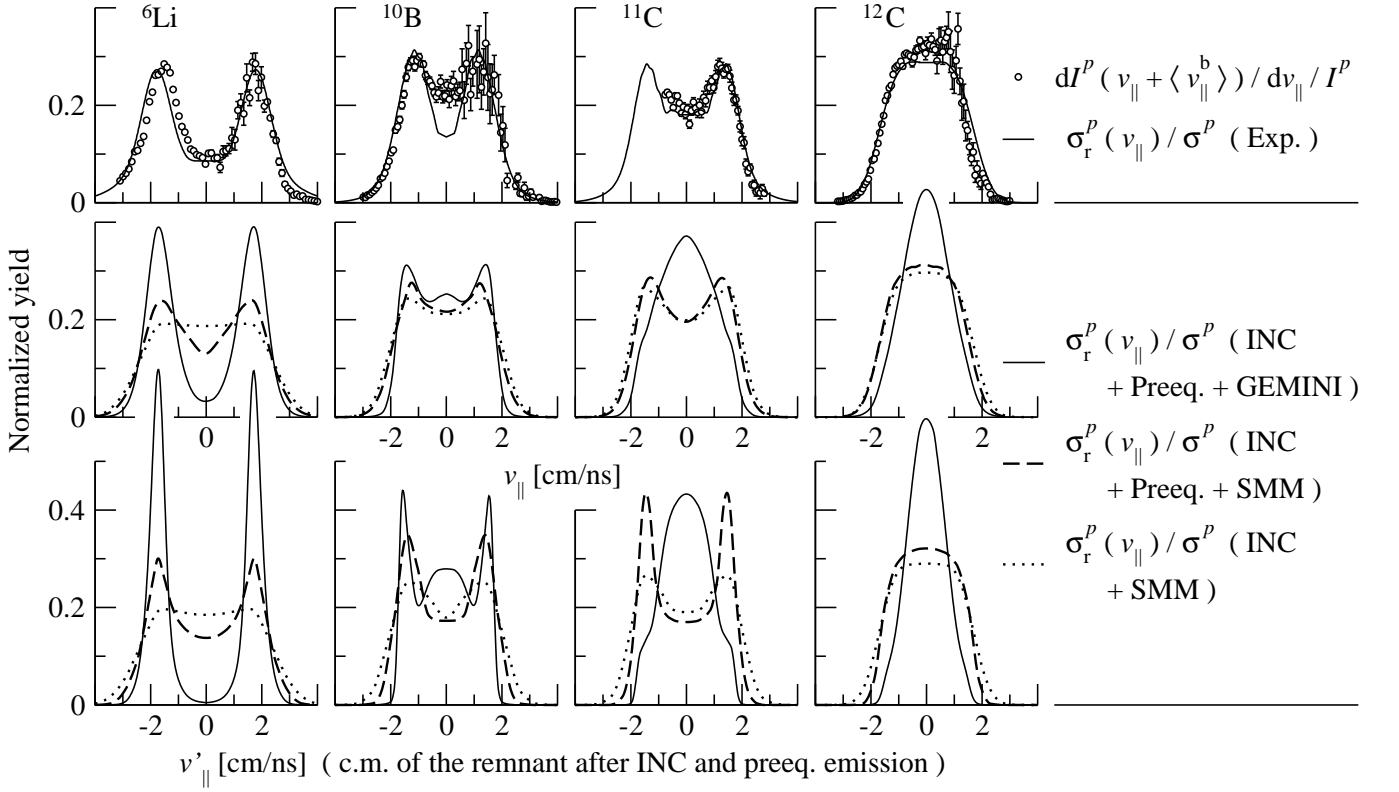


FIG. 16: *First row:* Experimental velocity spectra (circles) and reconstructed velocity spectra (solid line). Each spectrum is drawn in the reference frame corresponding to the measured average velocity value of the fragment considered. (This frame corresponds to the "center of mass" frame of the reaction product drawn in fig. 5) *Second row:* Calculated velocity spectra obtained by GEMINI or SMM following INC and the preequilibrium stage, and from SMM following directly INC. Each spectrum is drawn in the reference frame corresponding to the calculated average velocity value of the fragment considered. *Third row:* Velocity recoil introduced by the GEMINI or SMM phase alone (recoils by INC and preequilibrium stages not included). All spectra are normalized to the unit.

3. Fast break-up

We imputed the underestimation of intermediate-mass fragment formation to an incomplete description of the most highly excited decaying systems when solely fission-evaporation deexcitation was considered. In this respect, we turned to the Copenhagen-Moscow statistical multifragmentation model (SMM) [11, 13], that is the extension of the standard statistical evaporation-fission picture toward high excitation energies, treated by adding the fast simultaneous disassembly of the system as a possible decay channel. The hybrid model of intranuclear cascade followed by SMM was already applied in previous studies of proton-induced reactions [67, 68] for the description of similar experimental data. In the framework of SMM, the evaporation from the compound and compound-like nuclei is included and, therefore, at low excitation energies, if the channels with production of compound-like nuclei dominate, SMM gives results similar to GEMINI. In particular, the statistical cluster evaporation is treated within the Weisskopf formalism, extended to the emission of nuclei (in their ground state

or available excited states) up to ^{18}O [69]. On the other hand, when very high excitation energies are reached in the collision, the system is assumed to be diluted and to have attained the freeze-out density ρ_b . In previous studies [12] ρ_b was calculated to evolve as a function of the excitation energy per nucleon toward an almost asymptotic value equal to 1/3 of the ground-state density ρ_0 for high excitation energies ($E^*/A > 5$ MeV). In the present calculation, an energy-dependent free volume is used to determine the probability for different break-up partitions. On the other hand, for the calculation of the Coulomb interaction among fragments the freeze-out density ρ_b is introduced as a fixed quantity, equal to the asymptotic value $\rho_b = \rho_0/3$. According to the physical picture, when the region of phase (spinodal) instability is reached, at least partial thermodynamic equilibrium is expected and the fragment formation takes place according to chaotic oscillations among different break-up configurations, from event to event. In SMM, within the total accessible phase space, a microcanonical ensemble of all break-up configurations, composed of nucleons and excited intermediate-mass fragments governs the disas-

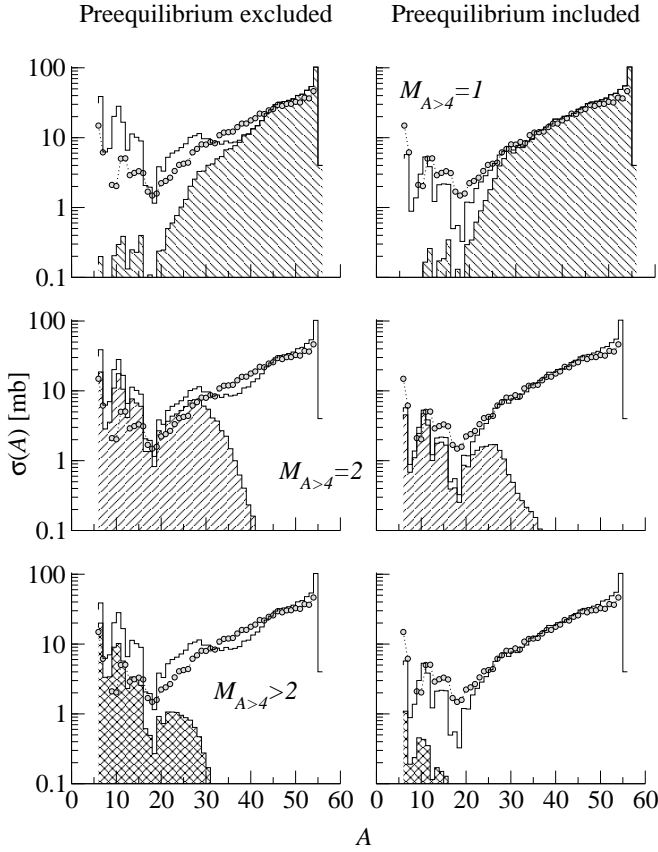


FIG. 17: The hatched areas represent portions of the residue production calculated with SMM, subdivided according to different multiplicities of intermediate-mass fragments (having $A > 4$). The total production measured experimentally (dots) and calculated (solid line) is superimposed for comparison. The calculation disregards preequilibrium in the left diagrams and includes preequilibrium in the right diagrams.

sembly of the hot remnant. The probability of different channels is proportional to their statistical weight. Several different break-up partitions of the system are possible.

In fig. 15, the calculation based on SMM reveals to better describe the reaction in comparison to GEMINI. It should also be observed that the production of intermediate-mass fragments is sensitive to the excitation energy of the source. A more detailed view on the reconstruction of the reaction mechanism is presented in fig. 17, where the multiplicities involved in the fragment formation are investigated. The major cross sections are fully determined by evaporation decays. This is true for the calculation where preequilibrium is included. On the contrary, when preequilibrium is excluded, a depletion of the heavy evaporation residues arises as a result of the excessive enhancement of higher-multiplicity modes (cluster emission and multifragmentation). The intermediate-mass fragments are almost totally produced in binary decays of mainly break-up character. Multifragment emis-

sion channels (with multiplicity mainly equal to three) have a minor contribution in the decay of the thermalised system but, when preequilibrium is disregarded, their incidence is in strong competition with binary splits. We might conclude that a consistent description of the production of fragments could be found in between these two approaches.

We can extend the investigation to the excitation energies connected to the production of fragments with different masses. According to the calculation presented in fig. 18 (now performed only including the preequilibrium phase), intermediate-mass fragments are almost all formed in the decay of highly excited remnants, with excitation energy per nucleon above 2.5 MeV.

An experimental indication of how multiplicity is related to the excitation energy is suggested by fig. 8 and the upper diagram of fig. 19, where the ratio of the sum of the individual production cross section in the two reactions and the total cross-section ratio are compared. The latter is calculated according to the model of Karol [70]. The production cross-section ratio scales with

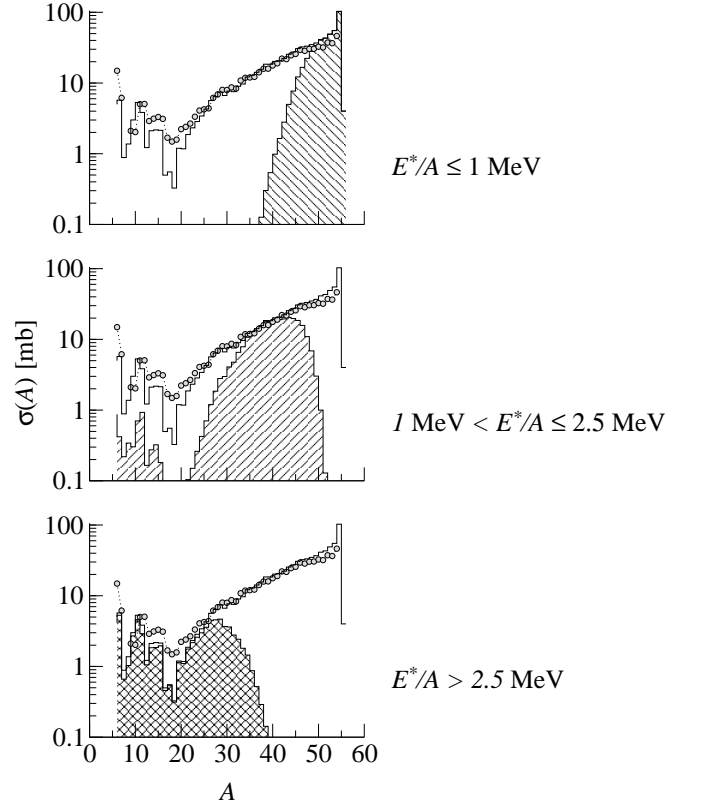


FIG. 18: Different portions (hatched areas) of the residue production calculated with SMM are selected according to different ranges in the excitation energy per nucleon E^*/A of the source. The calculation is performed only for the case of inclusion of preequilibrium. The total production measured experimentally (dots) and calculated (solid line) is superimposed for comparison.

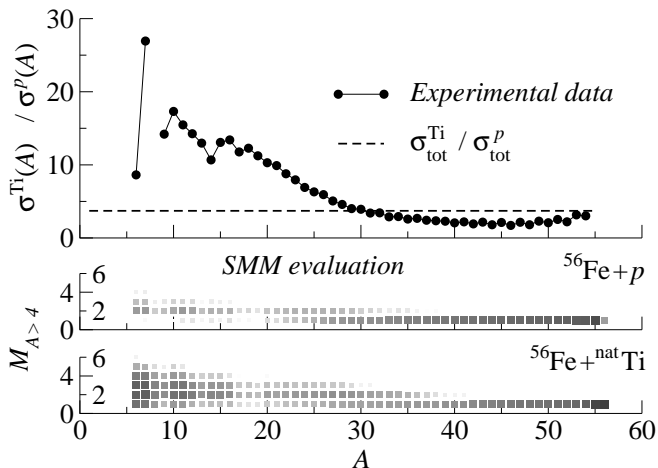


FIG. 19: *Upper part.* Experimental data on the production cross-sections ratio as a function of the mass number for the reaction $^{56}\text{Fe}+^{nat}\text{Ti}$ versus the reaction $^{56}\text{Fe}+p$. The data are compared with the ratio of total nuclear cross sections for the two reactions, calculated according to the model of Karol [70]. *Lower part.* SMM calculation of the probability for the formation of a residue as a function of the mass number and the multiplicity. The multiplicity is intended as the number of projectile-like residues heavier than an alpha particle produced in one collision.

the total cross-section ratio only in the region of higher masses, presumably coming from more peripheral collisions, while it deviates for lighter masses. The deviation must be related to the different mean multiplicities in the two reactions: lighter masses are more populated in the $^{56}\text{Fe}+^{nat}\text{Ti}$ reaction, and great part of this increase might be related to higher multiplicities. The observation of the gradual increase of multiplicity with the excitation of the system, verified in the calculation of different yield spectra associated to different energy ranges of hot remnants, could be followed further when extending to the $^{56}\text{Fe}+^{nat}\text{Ti}$ reaction. As pictured in the lower plots of fig. 19, this behaviour is well reproduced by calculations with SMM. In this respect, the light-residue production characterizing the $^{56}\text{Fe}+p$ system might just be interpreted as the early onset of the process that will govern the decay of the $^{56}\text{Fe}+^{nat}\text{Ti}$ system.

To conclude this section on model calculations, we focus once more on the velocity spectra of the light fragments shown in fig. 16. We already discussed the difficulty to combine the wide shapes of the velocity spectra and their mean values with a fission barrier. We inferred that the extensions of the velocity distributions to very high velocities might reflect higher kinetic energies than an asymmetric fission process could release. Consistently with this expectation, on the basis of model calculations we could connect the production of light residues to very high excitation energies of the source. Above around 2.5 MeV of excitation energy per nucleon, the process of light-residue production is still presumably dominated by

binary decays, but the contribution of disintegration in more fragments is not excluded. In this case, parts of the distribution corresponding to smaller velocities should be more populated than in a purely binary split. In the representation of fig. 16, this contribution would fill more central parts of the spectra when lower asymmetry characterizes the break-up partition. In a statistics of events where three about-equal-size fragments are produced simultaneously, the velocity spectrum of any of them will be Gaussian-like. If three fragments are produced, of which two are considerably lighter than their heavy partner, the velocity spectra σ_r of the two light ejectiles will be double humped. Another contribution in populating lower velocities could be associated to different break-up configurations, where the partner or the partners of the light residue have different masses. In this case, the spectrum is the folding of several binary-like components characterized by different spacing between the two maxima and different widths around the maxima, all this resulting in the superposition of two (backward and forward) triangular-like distributions that could eventually merge in a general bell-shape. We might also consider standard evaporation cooling down the break-up residues, emitted in some excited states. In this case, the secondary “slow” emission process operates outside of the common Coulomb field of the fragmenting remnant, and would produce a general widening of the spectrum around its maxima. As portrayed in the second row of fig. 16, SMM describes very consistently the experimental spectra. In the third row the effect of the Coulomb interaction and eventually the expansion is illustrated by referring to the center of mass of the system formed right after the intra-nuclear cascade and the pre-equilibrium, if included. SMM calculates the Coulomb interaction between fragments by placing them inside the freeze-out volume ρ_b . Contrarily to GEMINI, it takes into account different positions of the fragments, including two-body and many-body partitions. Some multi-fragmentation channels may resemble a two-body process even at relatively high excitation energy. These channels can also include additional small fragments which may look like evaporation ones. However, these additional small fragments can essentially change the Coulomb interaction in the volume and the thermal energy in the system, and influence the kinetic energies of the main two fragments. The binary character characterizing the experimental results is properly reproduced and the velocity distributions calculated with SMM are wider than those obtained from GEMINI. As shown in fig. 20, the gradual filling of the center of the spectra could be related to different break-up configurations and to possible multibody disintegration. The abrupt change of shape in passing from ^{11}C to ^{12}C (correctly reproduced by SMM) might be related to the more favoured evaporation channel toward the formation of ^{12}C , that could collect several different decay processes and evaporation decays from neighbouring nuclei. This preferential decay toward ^{12}C smears out any binary character of the spectrum. As

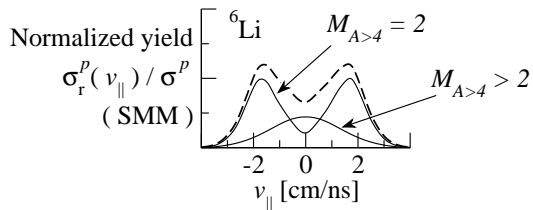


FIG. 20: Contribution of different multiplicity channels ($A>4$) to the velocity spectrum of ${}^6\text{Li}$, as calculated by SMM. The representation is the same as in the second column of fig. 16.

the break-up configuration varies with the mass and the charge of the end-product, it varies also with the excitation energy available for the disassembly of the hot remnant. This was evident in fig. 17, where we compared the production cross sections of the residues, and it is also evident in fig. 16, by analysing the velocity spectra. It is evident that the suppression of the preequilibrium induces a smearing effect on the spectra. This effect is dramatic for ${}^6\text{Li}$ as the double-humped spectrum is completely smeared out in one large single hump with a flat top, and it becomes similar to the velocity spectrum of ${}^6\text{Li}$ produced in the even more excited ${}^{56}\text{Fe}+{}^{\text{nat}}\text{Ti}$ system.

V. CONCLUSION

The mechanisms of light-particle emission from two systems, ${}^{56}\text{Fe}+p$ and ${}^{56}\text{Fe}+{}^{\text{nat}}\text{Ti}$ at 1 A GeV, have been investigated. The latter was regarded as a baseline for very high-energy processes (multifragmentation). We focused mainly on the proton-induced reaction. The certain understanding that we could attain from the analysis of the ${}^{56}\text{Fe}+p$ system is that light residues are produced in the decay of highly excited remnants. Furthermore, from a more quantitative discussion, we inferred that the emitting source should also be heavy and close to the projectile mass. The magnitude of the Coulomb repulsion, together with the very high formation yields even suggested that an asymmetric break-up process, hardly connected to asymmetric fission or statistical cluster emission, might be the favoured channel of light-residue production. These findings were derived from experimental observables like the isotopic cross sections measured for the whole ensemble of the residues, and the velocity distributions of the emitted fragments in the projectile frame along the beam axis. Especially the shape of the velocity spectra offered us a microscopic insight into the mechanisms of light-particle emission. In analysing the features of the velocity spectra, we failed in describing the kinematics within a general systematics of fission total-kinetic-energy release. A complete simulation of the whole reaction process, where sequential fission-evaporation decays govern the deexcitation, could not consistently describe the gross experimental features of

the decay.

We suggested that the characteristics of the kinematics and the production of light particles could carry indications of the complete reaction process, including channels of fast break-up decays revealed to be more adapted in depicting the decay of the most highly excited remnants, and was compatible with the high yields for light residues and the complex shapes of the velocity spectra. Encouraged by this consistency and, first of all, on the basis of previous theoretical and experimental results (see references in the section IV), we suggested that protons at incident energies of 1 A GeV traversing iron-like nuclei can introduce very high thermal excitation energy per nucleon in the system, even above 2.5 MeV. Such a thermal excitation could lead to attain freeze-out conditions.

We assume that if the excitation energy is high but not sufficient to lead to freeze-out, the system might still expand, but without reaching the break-up phase, the expansion subsequently reverses to compression in a path toward the formation of a compound nucleus. This behaviour might occur before the nucleus cools down by fission-evaporation decays. On the contrary, when the excitation energy is just sufficient to access break-up channels, partitions with low multiplicity of intermediate-mass fragments and high asymmetry are favoured: the decay results mainly in the simultaneous formation of one heavy residue, with mass close to the hot remnant, and one or more light clusters and nucleons. As an extreme case, two fragments rather asymmetric in mass may be formed in the same fast break-up process. The formation of light fragments in the ${}^{56}\text{Fe}+p$ reaction could be explained by this picture.

VI. ACKNOWLEDGMENTS

The experiment was performed in a joined effort by an international collaboration to provide new data for nuclear technology and for astrophysics. We thank our colleagues L. Audouin, C.-O. Bacri, J. Benlliure, B. Berthier, A. Boudard, E. Casarejos, J.J. Connell, S. Czajkowski, J.-E. Ducret, T. Enqvist, T. Faestermann, B. Fernandez, L. Ferrant, J.S. George, F. Hammache, A. Heinz, K. Helariutta, A.R. Junghans, B. Jurado, D. Karamanis, S. Leray, R.A. Mewaldt, M. Fernández Ordóñez, J. Pereira-Conca, M.V. Ricciardi, K. Sümmerer, C. Stéphan, C. Villagrasa, F. Vivès, C. Volant, M.E. Wiedenbeck, and N.E. Yanasak.

We are especially indebted to M. Bernas and P. Armbruster for sharing with us their expertise in the study of reaction kinematics and for enlightening explanations on the ion-optics of the FRagment Separator. We are grateful to A. Kelić and O. Yordanov for precious suggestions and remarks about the data analysis. The interpretation of our results profited from stimulating discussions with A. Boudard, C. Volant and S. Leray. We wish to thank F. Gulminelli for carefully reading the manuscript as well as

B. Borderie and J. P. Wieleczko for fruitful discussions. This work was supported by the European Union under the programme "Access to Research Infrastructure action of the Improving Human Potential" contract EC-HPR1-CT-1999-00001.

APPENDIX A: THE VELOCITY RECONSTRUCTION

1. Demonstration of the relation (3)

We describe hereafter the derivation of the equation (3), which connects the measured spectra $d\mathcal{I}(v_{\parallel})/dv_{\parallel}$ as a function of the longitudinal velocity component v_{\parallel} in the center-of-mass frame to the cross-section variation in velocity space in the center-of-mass frame. In a general case, the latter distribution is not isotropic, but a function of the absolute velocity v , the polar angle from the beam direction θ , and the azimuthal angle around the beam axis φ . It will be denoted as $d^3\sigma/(dv d\Omega)$, where Ω is the solid angle. The velocity component orthogonal to the beam axis is v_{\perp} . The contribution to the experimental yield in the interval $[v_{\parallel}, v_{\parallel} + \Delta v_{\parallel}]$ is obtained by integrating v_{\perp} in the slab orthogonal to the beam axis :

$$\frac{d\mathcal{I}(v_{\parallel})}{dv_{\parallel}} = \iint \frac{d^3\sigma}{d\vec{v}} v_{\perp} dv_{\perp} d\varphi \quad (\text{A1})$$

$$= \iint \frac{1}{v^2} \frac{d^3\sigma}{dv d\Omega} v_{\perp} dv_{\perp} d\varphi \quad (\text{A2})$$

For the orthogonal velocity integration the lower limit is 0 and the higher limit is related to the angular acceptance of the spectrometer. Since the latter is not necessarily circular, it can depend on φ and will be denoted as $\alpha(\varphi)$. The maximal orthogonal velocity may be derived from the Lorentz transformation of the momentum and it reads : $\tilde{v}_{\perp}(\varphi) = \gamma(u + v_{\parallel})\alpha(\varphi)$, where u and γ are the velocity and the Lorentz factor of the center of mass in the laboratory frame, respectively. Introducing these limits in the integration, we write :

$$\frac{d\mathcal{I}(v_{\parallel})}{dv_{\parallel}} = \int_0^{2\pi} \left[\int_0^{\tilde{v}_{\perp}(\varphi)} \frac{1}{v^2} \frac{d^3\sigma}{dv d\Omega} v_{\perp} dv_{\perp} \right] d\varphi \quad (\text{A3})$$

Changing the integration variable from v_{\perp} to $v = \sqrt{v_{\parallel}^2 + v_{\perp}^2}$ we obtain :

$$\frac{d\mathcal{I}(v_{\parallel})}{dv_{\parallel}} = \int_0^{2\pi} \left[\int_{|v_{\parallel}|}^{\sqrt{v_{\parallel}^2 + \tilde{v}_{\perp}^2(\varphi)}} \frac{1}{v} \frac{d^3\sigma}{dv d\Omega} dv \right] d\varphi \quad (\text{A4})$$

In the case of an isotropic velocity distribution, $d^3\sigma/(dv d\Omega)$ reduces to $(1/4\pi)(d\sigma/dv)$ which, substituted in eq. (A4) gives eq. (3).

2. Reversibility of the relation (3)

The physical quantity of interest in equation (3) is the term $d\sigma/dv$, describing the variation of the cross section $\sigma(v)$ as a function of the absolute velocity v in the center-of-mass frame, whereas the measured quantity is the left-hand term $d\mathcal{I}(v_{\parallel})/dv_{\parallel}$, representing the variation of the apparent cross section as a function of the longitudinal velocity component v_{\parallel} in the center-of-mass frame. In principle, equation (3) could not be inverted in an unambiguous way for general shapes of the $d\sigma/dv$ function. However, for the restricted shapes describing the data, this inversion becomes possible. This is particularly the case if this function is supposed to decrease monotonically to 0 at large v and if $d\mathcal{I}(v_{\parallel})/dv_{\parallel}$ also follows the same behaviour at large $|v_{\parallel}|$, as it is evident from fig. 3.

The inversion procedure can be described as follows. Let's consider a given bin in longitudinal velocity defined by the interval $[v_{\parallel}, v_{\parallel} + \Delta v_{\parallel}]$. The yield for this bin is $(d\mathcal{I}(v_{\parallel})/dv_{\parallel})/\Delta v_{\parallel}$, while the corresponding integral over v in equation (3) extends from v_{\parallel} to $\sqrt{v_{\parallel}^2 + v_{\perp}^2}$. This domain is depicted by the thick segment in fig. 21. Let us assume that the values of the function $d\sigma/dv$ are known over this interval and that they comply to equation (3).

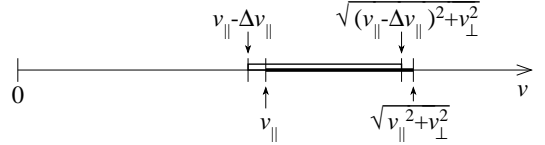


FIG. 21: Integration domains of eq. (3).

We consider now the v_{\parallel} bin located between $v_{\parallel} - \Delta v_{\parallel}$ and v_{\parallel} , for which the integration extends from $v_{\parallel} - \Delta v_{\parallel}$ and $\sqrt{(v_{\parallel} - \Delta v_{\parallel})^2 + v_{\perp}^2}$ as shown by the thin segment above the axis in fig. 21. It can be seen that this segment has a large overlap with the previous one, provided Δv_{\parallel} is small enough. If this were not the case, the inversion procedure would even be simplified as $d\sigma/dv$ would be directly proportional to the yield divided by the interval length, provided that the yield has a low variation over Δv_{\parallel} . In the case of overlap of the two integration segments, as shown in the figure, the variation of the yield comes only from the values of $d\sigma/dv$ at the edges. If the value is known on the right non-overlapping extremity, the variation between the two adjacent v_{\parallel} bins delivers the value on the left non-overlapping extremity. The procedure can be continued for lower v_{\parallel} bins, fixing the values of the function for decreasing values of v .

So far, no specific assumption has been made except that the function $d\sigma/dv$ is known over a given interval. This can be practically achieved if one assumes that $d\sigma/dv$ vanishes at large v values and that, as a consequence, also the yield drops. By considering a large v_{\parallel} value for which the yield is null, we can take a null $d\sigma/dv$

over the corresponding interval and start the procedure of reversion. This prescription for the starting point can also be extended to regions where the yield does not fade : for $v_{\parallel} \gg \tilde{v}_{\perp}$ the length of the integration interval decreases as $\tilde{v}_{\perp}^2/(2v_{\parallel})$, which becomes small compared to the characteristic variation length of $d\sigma/dv$. In this case, the latter can be assumed constant over the interval and its value deduced straightforward from eq. (3). The dependence of \tilde{v}_{\perp} on φ only slightly changes the procedure, while the scheme remains the same.

The yields measured for the forward emission ($v_{\parallel} > 0$) are expected to differ from those associated to the backward ($v_{\parallel} < 0$) emission. Nevertheless, in the ideal case of a perfectly isotropic emission with respect to the center of mass, the resulting cross sections $\sigma(v_{\parallel} > 0)$ and $\sigma(v_{\parallel} < 0)$ restricted to only-forward and only-backward emission, respectively, should be identical. The difference $|\sigma(v_{\parallel} > 0) - \sigma(v_{\parallel} < 0)|$ can be an indication of the uncertainty introduced in the extraction of the cross section $\sigma(v)$ by the assumption of isotropic emission.

APPENDIX B: ISOTOPIC CROSS SECTIONS

TABLE I: Spallation and fragmentation residue isotopic cross sections measured in this work for the formation of Li, Be, B, C, N and O in the reaction $^{56}\text{Fe}+p$ and $^{56}\text{Fe}+^{\text{nat}}\text{Ti}$, respectively.

Isotope	$^{56}\text{Fe}+p$, σ [mb]	$^{56}\text{Fe}+^{\text{nat}}\text{Ti}$, σ [mb]
^6Li	14.89 ± 1.5	128.50 ± 12.9
^7Li	3.06 ± 0.3	103.46 ± 10.3
^7Be	3.09 ± 0.3	62.28 ± 6.2
^9Be	2.11 ± 0.2	29.88 ± 3.0
^{10}B	2.03 ± 0.2	35.06 ± 3.5
^{11}B	3.82 ± 0.4	61.58 ± 6.2
^{12}B	0.36 ± 0.04	9.56 ± 1.0
^{11}C	1.12 ± 0.1	16.02 ± 1.6
^{12}C	4.69 ± 0.4	62.50 ± 6.3
^{13}C	2.76 ± 0.3	37.59 ± 3.6
^{14}C	1.87 ± 0.2	14.74 ± 1.5
^{13}N	0.14 ± 0.01	
^{14}N	1.25 ± 0.1	18.67 ± 1.9
^{15}N	2.97 ± 0.3	37.33 ± 3.7
^{16}N	0.33 ± 0.03	5.04 ± 0.5
^{17}N	0.11 ± 0.01	2.44 ± 0.2
^{18}N		0.01 ± 0.001
^{14}O	0.01 ± 0.001	
^{15}O	0.33 ± 0.03	5.91 ± 0.6
^{16}O	2.78 ± 0.3	36.62 ± 3.7
^{17}O	1.46 ± 0.1	15.58 ± 1.5
^{18}O	0.75 ± 0.08	9.12 ± 0.9
^{19}O	0.13 ± 0.01	1.99 ± 0.2

In the subsection IIB we described how cross sections could be extracted from the measured longitudinal velocity spectra. The results are presented in table I with the statistical uncertainties. In appendix A the numerical tool used in our analysis was presented. It should be observed that our velocity-reconstruction method allows to obtain cross sections for isotopes of which at least a half of the longitudinal velocity spectrum is measured. In this case, some needed parameters like the mean recoil velocity or the width of the distribution could be extrapolated from neighbouring isotopes. On the other hand, the whole procedure is valid up to a certain extent: due to the assumption of isotropic emission, ideal cases should result into equal (equal area and equal centroid) absolute-velocity distributions deduced from the forward and the backward part of the measured longitudinal velocity distributions. Deviations from this ideal case derive either from the physics of the reaction process, that could differ from a purely isotropic emission, or by the lack of statistics in some parts of the spectrum, resulting in complicating the convergence of the numerical calculation. This leads to results that fluctuate by 10% in the average. We take this value as the statistical uncertainty (and not simply the statistics of counts).

The systematic uncertainties are in general very small in FRS measurements of spallation residues. Indeed they rise to considerably high values when the measurement is dedicated to fragments having very high velocities in the projectile frame. This is the case of very light fragments emitted in fission-like events or in break-up processes. The largest source of uncertainty is the angular acceptance. Heavy residues, close to the projectile mass are emitted very forward, and the angular acceptance is close to 100%. On the contrary, light fragments are strongly affected. The multiplicity of the intermediate-mass fragments could not directly be measured. From physical arguments we could safely infer that light fragments are emitted in events with multiplicity (of fragments with $A > 4$) prevalently equal to two. Indeed we could not exclude the possible contribution of higher multiplicity processes. We estimated the systematic uncertainty to be up to 30%.

It might be remarked that the greatest contribution to the total uncertainty comes from the systematic uncertainty. On the other hand, the cross-section ratios of different nuclides are very consistent as they are related to small statistical uncertainties.

- [1] C. Villagrasa, A. Boudard, J.-E. Ducret, B. Fernandez, S. Leray, C. Volant, P. Armbruster, T. Enqvist, F. Hammache, K. Helariutta, B. Jurado, M.-V. Ricciardi, K.-H. Schmidt, K. Sümmerer, F. Vives, L. Audouin, L. Ferran, F. Rejmund, C. Stéphan, L. Tassan-Got, J. Benlliure, E. Casarejos, M. Fernandez, J. Pereira, S. Czajkowski, D. Karamanis, M. Pravikoff, J. George, R.A. Mewaldt, N. Yanasak, M. Wiedenbeck, J. Connell, T. Faestermann, A. Heinz, A. Junghans, Contr. to the Conference on Accelerator Applications in a Nuclear Renaissance (AccApp'03), San Diego, (USA), 2003.
- [2] "NEW MEASUREMENTS OF FRAGMENTATION CROSS SECTIONS FROM ^{56}Fe AND ^{60}Ni BEAMS AT ENERGIES RELEVANT TO GALACTIC COSMIC-RAY PROPAGATION". J.S. George, R.A. Mewaldt, N.E. Yanasak, M.E. Wiedenbeck, J.J. Connell, L. Audouin, C.-O. Bacri, B. Berthier, L. Ferrant, F. Rejmund, C. Stéphan, L. Tassan-Got, D. Karamanis, S. Czajkowski, A. Boudard, J.-E. Ducret, B. Fernandez, S. Leray, C. Villagrasa, C. Volant, T. Faestermann, T. Enqvist, F. Hammache, K. Helariutta, B. Jurado, K. H. Schmidt, K.Sümmerer, M.V. Ricciardi, F. Vivès, A. Heinz, J. Benlliure, E. Casarejos, M. Fernández Ordóñez, J. Pereira-Conca, and A.R. Junghans, Contr. to 27th International Cosmic Ray Conference, Hamburg (Germany), 2001.
- [3] C. Villagrasa et al., unpublished.
- [4] "BINARY DECAY OF LIGHT NUCLEAR SYSTEMS". S.J. Sanders, A. Szanto de Toledo, C. Beck, Phys. Rep. **311**, 487 (1999).
- [5] "STATISTICAL EMISSION OF LARGE FRAGMENTS: A GENERAL THEORETICAL APPROACH". L.G. Moretto, Nucl. Phys. A **247**, 211 (1975).
- [6] "THE CATEGORICAL SPACE OF FISSION". L.G. Moretto, G.J. Wozniak, Pramana - Journal of Physics **33**, 209 (1989).
- [7] "ON THE INTERPRETATION OF FISSION ASYMMETRY ACCORDING TO THE LIQUID DROP NUCLEAR MODEL". U.L. Businaro, S. Gallone, Nuovo Cimento **1**, 629 (1955).
- [8] "SADDLE SHAPES, THRESHOLD ENERGIES AND FISSION ASYMMETRY ON THE LIQUID DROP MODEL". U.L. Businaro, S. Gallone, Nuovo Cimento **1**, 1277 (1955).
- [9] "THE DISASSEMBLY OF NUCLEAR MATTER". J. Randrup, S.E. Koonin, Nucl. Phys. A **356**, 223 (1981).
- [10] "MICROCANONICAL THERMODYNAMICS AND STATISTICAL FRAGMENTATION OF DISSIPATIVE SYSTEMS. THE TOPOLOGICAL STRUCTURE OF THE N-BODY PHASE SPACE". D.H.E. Gross, Phys. Rep. **279**, 119 (1997).
- [11] "MULTIFRAGMENTATION OF NUCLEI AT EXCITATION ENERGIES 10 MEV/NUCLEON". A.S. Botvina, A.S. Iljinov, I.N. Mishustin, Yad. Fiz. **42**, 1127 (1985); Sov. J. Nucl. Phys., **42**, No. 5 712 (1985).
- [12] "STATISTICAL MULTIFRAGMENTATION OF NUCLEI". J.P. Bondorf, R. Donangelo, I.N. Mishustin, H. Schulz, Nucl. Phys. A **444**, 460 (1985).
- [13] "STATISTICAL MULTIFRAGMENTATION OF NUCLEI". J.P. Bondorf, A.S. Botvina, A.S. Iljinov, I.N. Mishustin, K. Sneppen, Phys. Rep. **257**, 133 (1995).
- [14] "A REEXAMINATION OF THE ABRASION-ABLATION MODEL FOR THE DESCRIPTION OF THE NUCLEAR FRAGMENTATION REACTION". J.-J. Gaimard, K.-H. Schmidt, Nucl. Phys. A **531**, 709 (1991).
- [15] "STATISTICAL ABRASION OF NUCLEONS FROM REALISTIC NUCLEAR-MATTER DISTRIBUTIONS". T. Brohm, K.-H. Schmidt, Nucl. Phys. A **569**, 821 (1994).
- [16] "MULTIFRAGMENTATION INDUCED BY LIGHT RELATIVISTIC PROJECTILES AND HEAVY IONS: SIMILARITIES AND DIFFERENCES". V.A. Karnaukhov, S.P. Avdeyev, W.D. Kuznetsov, L.A. Petrov, V.K. Rodionov, A.S. Zubkevich, H. Oeschler, O.V. Bochkarev, L.V. Chulkov, E.A. Kuzmin, A. Budzanowski, W. Karcz, M. Janicki, E. Norbeck, A.S. Botvina, Yad.Fiz. **62**, No 2, 2272 (1999); Phys. Atomic Nuclei **62**, 237 (1999).
- [17] "THERMAL MULTIFRAGMENTATION OF HOT NUCLEI AND LIQUID-FOG PHASE TRANSITION". V.A. Karnaukhov, S.P. Avdeyev, E.V. Duginova, L.A. Petrov, V.K. Rodionov, H. Oeschler, A. Budzanowski, W. Karcz, M. Janicki, O.V. Bochkarev, E.A. Kuzmin, L.V. Chulkov, E. Norbeck, A.S. Botvina, Yad.Fiz. **66**, 1282 (2003); Phys. Atomic Nuclei **66**, 1242 (2003).
- [18] "EXPERIMENTAL RESULTS FROM HIGH ENERGY PROTON-NUCLEUS INTERACTIONS, CRITICAL PHENOMENA, AND THE THERMAL LIQUID DROP MODEL OF FRAGMENT PRODUCTION". A.S. Hirsch, A. Bujak, J.E. Finn, L.J. Gutay, R.W. Minich, N.T. Porile, R.P. Scharenberg, and B.C. Stringfellow, F. Turkot, Phys. Rev. C **29**, 508 (1984).
- [19] "MASS YIELD DISTRIBUTIONS FOR 1 GEV PROTON-INDUCED NUCLEAR REACTIONS ON Ni AND Ag". L.N. Andronenko, A.A. Kotov, L.A. Vaishnena, W. Neubert, H.W. Barz, J.P. Bondorf, R. Donangelo, H. Schulz, Phys. Lett. B **174**, 18 (1986).
- [20] "INTERMEDIATE MASS FRAGMENT PRODUCTION ON Au, Ag, Ni AND Al TARGETS INDUCED BY 1 GEV PROTONS". A.A. Kotov, L.N. Andronenko, M.N. Andronenko, Y.I. Gusev, K.V. Lukashin, W. Neubert, D.M. Seliverstov, I.I. Strakovsky, L.A. Vaishnena, Nucl. Phys. A **583**, 575 (1995).
- [21] "THERMAL MULTIFRAGMENTATION IN $p + \text{Au}$ INTERACTIONS AT 2.16, 3.6 AND 8.1 GEV INCIDENT ENERGIES". S.P. Avdeyev, V.A. Karnaukhov, W.D. Kuznetsov, L.A. Petrov, V.K. Rodionov, A.S. Zubkevich, H. Oeschler, O.V. Bochkarev, L.V. Chulkov, E.A. Kuzmin, A. Budzanowski, W. Karcz, M. Janicki, E. Norbeck, A.S. Botvina, W.A. Friedman, W. Nörenberg, G. Papp, Eur. Phys. J. A **3**, 75 (1998).
- [22] "MICROSCOPIC MODEL APPROACHES TO FRAGMENTATION OF NUCLEI AND PHASE TRANSITIONS IN NUCLEAR MATTER". J. Richert and P. Wagner, Phys. Rep. **350**, 1 (2001).
- [23] "NUCLEAR SPINODAL FRAGMENTATION". P. Chomaz, M. Colonna, J. Randrup, Phys. Rep. **389**, 263 (2004).
- [24] "PROBING THE NUCLEAR LIQUID-GAS PHASE TRANSITION". J. Pochodzalla, T. Mohlenkamp, T. Rubehn, A. Schüttauf, A. Worner, E. Zude, M. Begemann-Blaich, T. Blaich, H. Emling, A. Ferrero, C. Gross, G. Imme, I. Iori,

- G.J. Kunde, W.D. Kunze, V. Lindenstruth, U. Lynen, A. Moroni, W.F.J. Müller, B. Ocker, G. Raciti, H. Sann, C. Schwarz, W. Seidel, V. Serfling, J. Stroth, W. Trautmann, A. Trzcinski, A. Tucholski, G. Verde, B. Zwieglinski, *Phys.Rev.Lett.* **75**, 1040 (1995).
- [25] "DYNAMICS AND THERMODYNAMICS OF THE LIQUID-GAS PHASE TRANSITION IN HOT NUCLEI STUDIED WITH THE INDRA ARRAY".
B. Borderie, *J. Phys. (London) G* **28**, R217 (2002).
- [26] "THERMAL PROPERTIES OF NUCLEI".
G. Sauer, H. Chandra, U. Mosel, *Nucl. Phys. A* **264**, 221 (1976).
- [27] "NUCLEAR CONDENSATION".
H. Jaqaman, A.Z. Mekjian, L. Zamick, *Phys.Rev. C* **27**, 2782 (1983).
- [28] "COULOMB INSTABILITY IN HOT COMPOUND NUCLEI APPROACHING LIQUID-GAS TRANSITION".
S. Levit, P. Bonche, *Nucl. Phys. A* **437**, 426 (1985).
- [29] "LIQUID TO VAPOR PHASE TRANSITION IN EXCITED NUCLEI".
J.B. Elliott, L.G. Moretto, L. Phair, G.J. Wozniak, L. Beaulieu, H. Breuer, R.G. Korteling, K. Kwiatkowski, T. Lefort, L. Pienkowski, A. Ruangma, V.E. Viola, S.J. Yennello, and the ISiS Collaboration, *Phys.Rev.Lett.* **88**, 042701 (2002).
- [30] "CRITICAL TEMPERATURE FOR THE NUCLEAR LIQUID-GAS PHASE TRANSITION".
V.A. Karnaukhov, H. Oeschler, S.P. Avdeyev, E.V. Duginova, V.K. Rodionov, A. Budzanowski, W. Karcz, O.V. Bochkarev, E.A. Kuzmin, L.V. Chulkov, E. Norbeck, A.S. Botvina, *Phys.Rev. C* **67**, 011601 (2003).
- [31] "LITTLE BIG BANG SCENARIO OF MULTIFRAGMENTATION".
X. Campi, H. Krivine, E. Plagnol, N. Sator, *Phys.Rev. C* **67**, 044610 (2003).
- [32] "COULOMB INSTABILITY OF HOT NUCLEI".
H.R. Jaqaman, *Phys.Rev. C* **39**, 169 (1989).
- [33] "INSTABILITY OF HOT NUCLEI".
H.R. Jaqaman, *Phys.Rev. C* **40**, 1677 (1989).
- [34] "STATISTICAL MULTIFRAGMENTATION IN THERMODYNAMIC LIMIT".
K.A. Bugaev, M.I. Gorenstein, I.N. Mishustin, W. Greiner *Phys.Lett. B* **498**, 144 (2001)
- [35] "PRODUCTION OF NEUTRON-RICH HEAVY RESIDUES AND THE FREEZE-OUT TEMPERATURE IN THE FRAGMENTATION OF RELATIVISTIC ^{238}U PROJECTILES DETERMINED BY THE ISOSPIN THERMOMETER".
K.-H.Schmidt, M.V.Ricciardi, A.S.Botvina, T.Enqvist, *Nucl. Phys. A* **710**, 157 (2002).
- [36] "DETERMINATION OF THE FREEZE-OUT TEMPERATURE BY THE ISOSPIN THERMOMETER".
P. Napolitani, K.-H. Schmidt, P. Armbruster, A.S. Botvina, M.V. Ricciardi, L. Tassan-Got, F. Rejmund, T. Enqvist, *Yad.Fiz.* **66**, No. 8, 1517 (2003); *Phys. Atomic Nuclei* **66**, No. 8, 1471 (2003).
- [37] "BASIS FOR A CHARACTERISTIC TEMPERATURE IN NUCLEAR FRAGMENTATION".
W.A. Friedman, *Phys.Rev.Lett.* **60**, 2125 (1988).
- [38] "UNIVERSALITY OF SPECTATOR FRAGMENTATION AT RELATIVISTIC BOMBARDING ENERGIES".
A. Schüttauf, W.D. Kunze, A. Worner, M. Begemann-Blaich, Th. Blaich, D.R. Bowman, R.J. Charity, A. Cosmo, A. Ferrero, C.K. Gelbke, C. Gross, W.C. Hsi, J. Hubele, G. Imme, I. Iori, J. Kempter, P. Kreutz, G.J. Kunde, V. Lindenstruth, M.A. Lisa, W.G. Lynch, U. Lynen, M. Mang, T. Mohlenkamp, A. Moroni, W.F.J. Müller, M. Neumann, B. Ocker, C.A. Ogilvie, G.F. Peaslee, J. Pochodzalla, G. Raciti, F. Rosenberger, Th. Rubehn, H. Sann, C. Schwarz, W. Seidel, V. Serfling, L.G. Sobotka, J. Stroth, L. Stuttge, S. Tomasevic, W. Trautmann, A. Trzcinski, M.B. Tsang, A. Tucholski, G. Verde, C.W. Williams, E. Zude, B. Zwieglinski, *Nucl.Phys. A* **607**, 457 (1996).
- [39] "EXPERIMENTAL DETERMINATION OF FRAGMENT EXCITATION ENERGIES IN MULTIFRAGMENTATION EVENTS".
N. Marie, A. Chbihi, J.B. Natowitz, A. Le Fevre, S. Salou, J.P. Wieleczko, L. Gingras, M. Assenard, G. Auger, Ch.O. Bacri, F. Bocage, B. Borderie, R. Bougault, R. Brou, P. Buchet, J.L. Charvet, J. Cibor, J. Colin, D. Cusol, R. Dayras, A. Demeyer, D. Dore, D. Durand, P. Eudes, J.D. Frankland, E. Galichet, E. Genouin-Duhamel, E. Gerlic, M. Germain, D. Gourio, D. Guinet, K. Hagel, P. Lantesse, J.L. Laville, J.F. Lecolley, T. Lefort, R. Legrain, N. Le Neindre, O. Lopez, M. Louvel, Z. Majka, A.M. Maskay, L. Nalpas, A.D. Nguyen, M. Parlog, J. Peter, E. Plagnol, A. Rahmani, T. Reposeur, M.F. Rivet, E. Rosato, F. Saint-Laurent, J.C. Steckmeyer, M. Stern, G. Tabacaru, B. Tamain, O. Tirel, E. Vient, C. Volant, R. Wada, *Phys.Rev. C* **58**, 256 (1998).
- [40] "COMPARISON OF 1 A GeV $^{197}\text{Au} + \text{C}$ DATA WITH THERMODYNAMICS: THE NATURE OF THE PHASE TRANSITION IN NUCLEAR MULTIFRAGMENTATION".
R.P. Scharenberg, B.K. Srivastava, S. Albergo, F. Bieser, F.P. Brady, Z. Caccia, D.A. Cebra, A.D. Chacon, J.L. Chance, Y. Choi, S. Costa, J.B. Elliott, M.L. Gilkes, J.A. Hauger, A.S. Hirsch, E.L. Hjort, A. Insolia, M. Justice, D. Keane, J.C. Kintner, V. Lindenstruth, M.A. Lisa, H.S. Matis, M. McMahan, C. McParland, W.F. J. Müller, D.L. Olson, M.D. Partlan, N.T. Porile, R. Potenza, G. Rai, J. Rasmussen, H.G. Ritter, J. Romanowski, J.L. Romero, G.V. Russo, H. Sann, A. Scott, Y. Shao, T.J.M. Symons, M. Tincknell, C. Tuvé, S. Wang, P. Warren, H.H. Wieman, T. Wienold, K. Wolf (EOS Collaboration), *Phys.Rev. C* **64**, 054602 (2001).
- [41] "TRANSITION FROM FISSION TO MULTIFRAGMENTATION".
G. Klotz-Engmann, H. Oeschler, E. Kankeleit, Y. Casagnou, M. Conjeaud, R. Dayras, S. Harar, M. Mostefai, R. Legrain, E.C. Pollacco, C. Volant, *Phys. Lett.* **187 B**, 245 (1987).
- [42] "PROPERTIES OF BINARY FISSION AND MULTIFRAGMENTATION IN THE TRANSITION REGIME".
G. Klotz-Engmann, H. Oeschler, J. Stroth, E. Kankeleit, Y. Cassagnou, M. Conjeaud, R. Dayras, S. Harar, R. Legrain, B.C. Pollacco, C. Volant, *Nucl. Phys. A* **499** 392 (1989)
- [43] "THE GSI PROJECTILE FRAGMENT SEPARATOR (FRS): A VERSATILE MAGNETIC SYSTEM FOR RELATIVISTIC HEAVY IONS".
H. Geissel, P. Armbruster, K.H. Behr, A. Brünle, K. Burkard, M. Chen, H. Folger, B. Franczak, H. Keller, O. Klepper, B. Langenbeck, F. Nickel, E. Pfeng, M. Pfützner, E. Roeckl, K. Rykaczewski, I. Schall, D. Schardt, C. Scheidenberger, K.-H. Schmidt, A. Schroter, T. Schwab, K. Stümmerer, M. Weber, G. Münzenberg, T. Brohm, H.-G. Clerc, M. Fauerbach, J.-J. Gaimard, A. Grewe, E. Hanelt, B. Knödler, M. Steiner, B. Voss, J. Weckenmann, C. Ziegler, A. Magel, H. Wollnik, J.P. Du-

- four, Y. Fujita, D.J. Vieira, B. Sherrill, *Nucl. Instrum. Methods B* **70**, 286 (1992). *Nucl. Instrum. Methods B* **70**, 286 (1992).
- [44] P. Napolitani, "MEASUREMENT OF SPALLATION RESIDUES OF THE REACTION $^{56}\text{Fe}+p$ AT 1 A GeV, ". DEA-report, IPN-Orsay (2001).
- [45] "NEW APPROACH TO DETERMINE THE ANGULAR TRANSMISSION IN ZERO-DEGREE MAGNETIC SPECTROMETERS". J. Benlliure, J. Pereira-Conca, K.-H. Schmidt, *Nucl. Instrum. Methods. A* **478**, 493 (2002).
- [46] "ISOTOPIC PRODUCTION CROSS SECTIONS OF FISSION RESIDUES IN ^{197}Au -ON-PROTON COLLISIONS AT 800 A MeV". J. Benlliure, P. Armbruster, M. Bernas A. Boudard, J. P. Dufour, T. Enqvist, R. Legrain, S. Leray, B. Mustapha, F. Rejmund, K.-H. Schmidt, C. Stéphan, L. Tassan-Got, C. Volant, *Nucl. Phys. A* **683**, 513 (2001).
- [47] "ISOTOPIC YIELDS AND KINETIC ENERGIES OF PRIMARY RESIDUES IN 1 A GeV $^{208}\text{Pb} + p$ REACTIONS". T. Enqvist, W. Wlazole, P. Armbruster, J. Benlliure, M. Bernas, A. Boudard, S. Czajkowski, R. Legrain, S. Leray, B. Mustapha, M. Pravikoff, F. Rejmund, K.-H. Schmidt, C. Stephan, J. Taieb, L. Tassan-Got, C. Volant, *Nucl. Phys. A* **686**, 481 (2001).
- [48] "FISSION RESIDUES PRODUCED IN THE SPALLATION REACTION $^{238}\text{U}+p$ AT 1 A GeV". M. Bernas, P. Armbruster, J. Benlliure, A. Boudard, E. Casajeros, S. Czajkowski, T. Enqvist, R. Legrain, S. Leray, B. Mustapha, P. Napolitani, J. Pereira, F. Rejmund, V. Ricciardi, K.-H. Schmidt, C. Stéphan, J. Taieb, L. Tassan-Got, C. Volant, *Nucl. Phys. A* **725**, 213 (2003).
- [49] "SYSTEMATICS OF MOMENTUM DISTRIBUTIONS FOR REACTIONS WITH RELATIVISTIC IONS". D.J. Morrissey, *Phys. Rev. C* **39**, 460 (1989).
- [50] "LIGHT FRAGMENT EMISSION AS STUDIED BY THE (P,PHE) REACTIONS ON BE AND AG WITH 300 MEV PROTONS". R.G. Korteling, R.E.L. Green, J.M. D'Auria, R.L. Helmer, K.P. Jackson, S.B. Kaufman, B.D. Wilkins, *Phys. Rev. C* **41**, 2571 (1990).
- [51] "SYSTEMATICS OF COMPLEX FRAGMENT EMISSION IN NIOBIUM-INDUCED REACTIONS". R. Babinet. These, Université de Paris Sud, Orsay (1981)
- [52] "TIME SCALE FOR EMISSION OF SOFT EJECTILES IN THE DISASSEMBLY OF HOT NUCLEI". G. Wang, K. Kwiatkowski, D.S. Bracken, E. Renshaw Foxford, W.-C. Hsi, R.G. Korteling, R. Legrain, K.B. Morley, E.C. Pollacco, V.E. Viola, C. Volant, *Phys. Rev. Lett. C* **57**, R2786 (1998).
- [53] "SOURCE SIZE AND TIME DEPENDENCE OF MULTIFRAGMENTATION INDUCED BY GeV ^3He BEAMS". G. Wang, K. Kwiatkowski, D.S. Bracken, E. Renshaw Foxford, W.-C. Hsi, K.B. Morley, V.E. Viola, N.R. Yoder, C. Volant, R. Legrain, E.C. Pollacco, R.G. Korteling, W.A. Friedman, A. Botvina, J. Brzychczyk, H. Breuer, *Phys. Rev. C* **60**, 014603 (1999).
- [54] "SYMMETRIC SPLITTING OF VERY LIGHT SYSTEMS". K. Grotowski, Z. Majka, R. Planeta, M. Szczodrak, Y. Chan, G. Guarino, L.G. Moretto, D.J. Morrissey, L.G. Sobotka, R.G. Stokstad, I. Tserruya, S. Wald, G.J. Wozniak, *Phys. Rev. C* **30**, 1214 (1984).
- [55] "SYSTEMATICS OF FISSION FRAGMENT TOTAL KINETIC ENERGY RELEASE". V.E. Viola, K. Kwiatkowski, M. Walker, *Phys. Rev. C* **31**, 1550 (1985).
- [56] "A NEW SYSTEMATICS OF FRAGMENT TOTAL KINETIC ENERGY RELEASE IN FISSION". O.A.P. Tavares, M.L. Terranova, *Nuovo Cim. A* **105**, 723 (1992).
- [57] "ONSET OF MULTIFRAGMENTATION DOMINANCE AT 1 GeV PROTON-INDUCED NUCLEAR REACTION FOR TARGET NUCLEI WITH $A \leq 160$ ". H.W. Barz, J.P. Bondorf, H. Schulz, L.N. Andronenko, A.A. Kotov, L.A. Vaishnena, W. Neubert, *Nucl. Phys. A* **460**, 714 (1986).
- [58] "STATISTICAL MODEL OF FRAGMENTATION PROCESSES". A.S. Goldhaber, *Phys. Lett. B* **53**, 306 (1974).
- [59] "ENERGY SPECTRA OF NUCLEAR FRAGMENTS PRODUCED BY HIGH ENERGY PROTONS". G.D. Westfall, R.G. Sextro, A.M. Poskanzer, A.M. Zebelman, G.W. Butler, E.K. Hyde *Phys. Rev. C* **17**, 1368 (1978).
- [60] "FRAGMENT KINETIC ENERGIES AND MODES OF FRAGMENT FORMATION". T. Odeh, R. Bassini, M. Begemann-Blaich, S. Fritz, S. J. Gaff-Ejakov, D. Gourio, C. Gross, G. Immé, I. Iori, U. Kleinevoss, G. J. Kunde, W. D. Kunze, U. Lynen, V. Maddalena, M. Mahi, T. Möhlenkamp, A. Moroni, W. F. J. Müller, C. Nociforo, B. Ocker, F. Petruzzelli, J. Pochodzalla, G. Raciti, G. Riccobene, F. P. Romano, A. Saija, M. Schnittker, A. Schüttauf, C. Schwarz, W. Seidel, V. Serfling, C. Sienti, W. Trautmann, A. Trzcinski, G. Verde, A. Wörner, Hongfei Xi, B. Zwieglinski, *Phys. Rev. Lett.* **84**, 4557 (2000).
- [61] "EVIDENCE FOR A BLAST WAVE FROM COMPRESSED NUCLEAR MATTER". P.J. Siemens, J.O. Rasmussen, *Phys. Rev. Lett.* **42**, 880 (1979).
- [62] "VARIATION OF THE COULOMB REPLUSION IN MULTIFRAGMENTATION". H. Oeschler, A.S. Botvina, D.H.E. Gross, S.P. Avdeyev, V.A. Karnaukhov, L.A. Petrov, V.K. Rodionov, O.V. Bochkarev, L.V. Chulkov, E.A. Kuzmin, A. Budzanowski, W. Karcz, M. Janicki, E. Norbeck, *Physics of Particles and Nuclei Lett* **99**, 70 (2000).
- [63] "CASCADE-EXCITON MODEL OF NUCLEAR REACTIONS". K.K. Gudima, S.G. Mashnik, V.D. Toneev, *Nucl. Phys. A* **401**, 329 (1983).
- [64] "STATISTICAL MODEL OF INTERMEDIATE STRUCTURE". J.J. Griffin, *Phys. Rev. Lett.* **17**, 478 (1966).
- [65] "HYBRID MODEL FOR PRE-EQUILIBRIUM DECAY IN NUCLEAR REACTIONS". M.Blann, *Phys. Rev. Lett.* **27**, 337 (1971).
- [66] "SYSTEMATICS OF COMPLEX FRAGMENT EMISSION IN NIOBIUM-INDUCED REACTIONS". R.J. Charity, M.A. McMahan, G.J. Wozniak, R.J. McDonald, L.G. Moretto, D.G. Sarantites, L.G. Sobotka, G. Guarino, A. Pantaleo, L. Fiore, A. Gobbi, K.D. Hildenbrand, *Nucl. Phys. A* **483**, 371 (1988).
- [67] "MULTIFRAGMENTATION OF NUCLEI BY HIGH-ENERGY PROTONS". A.S. Botvina, A.S. Iljinov, I.N. Mishustin, *JETP Lett.* **42**, 572 (1985).
- [68] "MULTIFRAGMENT BREAK-UP OF NUCLEI BY INTERMEDIATE-ENERGY PROTONS". A.S. Botvina, A.S. Iljinov, I.N. Mishustin, *Nucl. Phys. A* **507**, 649 (1990).
- [69] "STATISTICAL SIMULATION OF THE BREAK-UP OF HIGHLY

EXCITED NUCLEI”.

A.S. Botvina, A.S. Iljinov, I.N. Mishustin, J.P. Bondorf, R. Donangelo, K. Sneppen, Nucl. Phys. A **475**, 663 (1987).

[70] “NUCLEUS-NUCLEUS REACTION CROSS SECTIONS AT HIGH ENERGIES: SOFT-SPHERE MODEL”.

P.J. Karol, Phys. Rev. C **11**, 1203 (1975). Proceeding of Symposium on the Hahn-Meitner-Institut für Kernforschung, Berlin (1979).